IEEE Access
Multidisciplinary | Rapid Review | Open Access Journal

Received May 18, 2019, accepted May 24, 2019, date of publication May 31, 2019, date of current version June 19, 2019.

Digital Object Identifier 10.1109/ACCESS.2019.2920244

Adaptive Cooperative Non-Orthogonal Multiple Access-Based Power Line Communication

HONGHONG PU, (Student Member, IEEE), XIAOSHENG LIU, (Member, IEEE), SHU ZHANG, (Student Member, IEEE), AND DIANGUO XU, (Fellow, IEEE)
School of Electrical Engineering and Automation, Harbin Institute of Technology, Harbin 15001, China

Corresponding author: Xiaosheng Liu (liuxsh2004@126.com)

This work was supported in part by the National Natural Science Foundation of China under Grant 51677034, and in part by the Natural Science Foundation of Heilongjiang Province of China under Grant ZD2018012.

ABSTRACT This paper proposes an adaptive cooperative non-orthogonal multiple access (NOMA) scheme for power line communication (PLC) networks, in which the source superimposes the data symbols to two users. Specifically, the source communicates with the far-user with the assistance of relay. Meanwhile, depending on negligible 1-bit feedback, the near-user is reached through an adaptive way which switches between a direct and a cooperative data transmission mode, resulting in an enhancement of the system throughput and a more reliable data reception at the near-user. For this setting, we then analyze the system throughput over the log-normal distributed channel fading with the impulsive noise and investigate the impact of key system parameters. The simulation results validate the theoretical analysis and show that our scheme can obtain a better throughput performance with lower power consumption and reduce the electromagnetic compatibility (EMC) issues for PLC networks more efficiently than the time division multiple access (TDMA) and traditional cooperative NOMA (TCN) schemes.

INDEX TERMS Power line communication (PLC), non-orthogonal multiple access (NOMA), log-normal distribution, impulsive noise, system throughput.

I. INTRODUCTION

The Internet of Things (IoT) is regarded as a very promising digital communication system and widely applied in sensors, smart devices, smart metering, and control systems [1], [2]. The communication techniques play a key role in combing all the sensors, actuators, management systems, and databases together to fulfill the needs and demands of IoT. In general, wireless communication is adopted as the main method of communication in IoT. However, with the rapid development of smart grid (SGs) and power energy internets (EGs), the important areas in IoT, power line communication (PLC) has become an attractive communication method for IoT, since it has advantages of easy installation and cost efficiency [2], [3]. In addition, PLC network are envisioned as an integral part of future 5G networks to provide wireline backhaul for wireless access points [4]. However, there exist many practical challenges that impair the communication reliability over a PLC channel, such as the impulsive noise, impedance mismatch, multipath fading, frequency/distance dependent attention, and electromagnetic compatibility (EMC) issues [5]–[8].

Cooperative relaying is an efficient way to diminish the impact of the harsh and hostile PLC environment and offers a considerable throughput improvement and range extension [9]–[16]. More specifically, Cheng *et al.* [9] investigated an Amplify-and-forward (AF) based relay-aided PLC system. Through the optimal power allocation, this scheme can provided a considerable capacity improvements than direct-link PLC. Ezzine *et al.* [12] analyzed channel capacity for AF, decode-and-forward (DF) and fountain-code and forward (FCF) protocol for orthogonal frequency-division multiplexing (OFDM) based dual-hop relaying PLC systems. Facina *et al.* [13] analyzed AF and DF PLC together with three combining techniques, i.e., election combining (SC), equal gain combining (EGC) and maximum ratio combining (MRC). Besides, recently, Rabie *et al.*, [14], Rabie and Adebisi [15] proposed the energy-harvesting schemes for relaying PLC networks and demonstrated that an enhancement of capacity can be achieved. Qian *et al.*, [16]

The associate editor coordinating the review of this manuscript and approving it for publication was Zhen Li.

proposed an opportunistic DF-based multiple-relaying scheme to enhance the performance of PLC networks, where the optimal relay was selected dynamically. A common feature of the aforementioned works is that either time division multiple access (TDMA) or OFDM is adopted to accomplish data transmissions between PLC modems, which is essentially orthogonal multiple access (OMA). The enhancement of data reception reliability at receiver brought by OMA comes at the price of reduced spectral efficiency due to the additional time or frequency resource used for cooperation.

To overcome this issue, non-orthogonal multiple access (NOMA), the promising multiple access candidate of future radio access networks, which allows simultaneous data transmission for different users (i.e., modems) at the same time and frequency with different power levels [17], [18], was recently introduced in cooperative PLC networks [19], [20]. Cooperative NOMA PLC networks can not only improve the system capacity, spectral efficiency and fairness between different users, but relax the EMC issues, resulting a better coexistence with wireless networks [19]. More specifically, Rabie*et al*. [19] analyzed the average sum capacity performance of NOMA based dual hop cooperative relaying PLC system adopting DF protocol, achieving a superior capacity performance compared with conventional cooperative relaying PLC system. An improved cooperative NOMA scheme was proposed in [20] by implementing NOMA at both source and relay. Compared with [19], where NOMA was only deployed at source, this scheme can obtain a significant gains in the average capacity. It is worthwhile to point out that a high throughput may leads to time delay during data transmission, although it is not the concerns of this paper. The balance between the high throughput requirement and the stringent latency requirements is needed, especially in a delay-sensitive application, such as the monitoring application of smart grids [21] and power system [22].

The aforementioned works on cooperative NOMA usually assume that users cannot communicate with source without the assistance of relay. A more typical scenario of cooperative relaying networks, in which the near-user can directly communicates with source while the far-user is reached through a dedicated relay, however, has been investigated in wireless networks [23]–[26]. Besides, recall that the incremental relaying, which allows a relay for cooperation only when the channel quality from source to destination is below a given threshold, achieves a significant enhancement of spectral efficiency [27], [28]. More specifically, a negligible 1-bit feedback was introduced for indicating whether the destination node correctly decode its desired signal, i.e., a 1-bit positive feedback is transmitted by the destination node to the source when the desired signal was decoded correctly; otherwise, a 1-bit negative feedback was transmitted. This scheme is essentially an adaptive scheme which can adaptively switches the relay on or off depending on the feedback from destination. Motivated by this feature, this paper focuses on the similar network scenario adopted in [23]–[26] and proposes an adaptive cooperative NOMA (ACN) scheme for PLC networks. In this scheme, the far-user communicates with source with the assistance of a relay, while the near-user communicates with source in an adaptive way, which switches between a direct and a cooperative transmission mode. Specifically, if the near-user can correctly decode its desired signal during the first phase, it feeds back a 1-bit positive acknowledge (ACK) to the source; otherwise, a 1-bit negative ACK (NACK) is transmitted by the near-user to the source. If the ACK feedback is received, the source will also participate in the second phase's data transmission and sends a new data symbol to the near-user through the direct link transmission. However, if the NACK feedback is received, the source will keep silent and the near-user will attempt to retrieve its desired signal by overhearing the signal forwarded by relay during the second phase. In this way, additional data rates and more reliable data reception at the near-user can be obtained.

The main contributions of this paper as follows. We first proposed an adaptive cooperative NOMA scheme with considering a more typical cooperative network scenario. Then we analyze the system performance in term of the system throughput and investigate the impact of key system parameters, such as the occurrence probability of impulsive noise, power allocation coefficients, and source and relay transmit signal-to-noise ratio (SNR). Simulation results are finally provided to verify the accuracy of the theoretical analysis and reveal that the achievable performance of the proposed ACN scheme is superior to that of two benchmark schemes, i.e., the TDMA and traditional cooperative NOMA (TCN) scheme. It should be noted that this paper assumes that the amplitude of PLC channel fading coefficient follows log-normal distribution, and that the frequency/distance dependent attenuation is denoted by Zimmermann and Dostert's model [14], [15], [19], [20], [29], [30].

The rest of this paper is organized as follows. In Section II, we illustrate the system model of our ACN scheme and two benchmark schemes. Section III analyzes the corresponding system throughput. Simulation results are presented in Section IV. Section V concludes this paper.

The following notation are used hereafter. The notation $|\cdot|$ is the magnitude operator and $E[\cdot]$ is the statistical expectation. The notations $f(\cdot)$, $F(\cdot)$ and $\overline{F}(\cdot)$ respectively represent the probability density function (PDF), cumulative distribution function (CDF), and complementary CDF (CCDF).

II. SYSTEM MODEL

In this section, we first describe the system model of the ACN scheme and then present that of two benchmark schemes.

Fig.1 shows a basic model of downlink cooperative NOMA based PLC system which consists of four PLC modems: a source S, a relay R, a near-user D1 and a far-user D2. It is assumed that the direct transmission link between S and D2 does not exist due to deep fading, while S can directly communicate with D1. Each modem operates in half-duplex mode and a DF protocol is adopted at R. The channel fading coefficients from S to D1 and D2, from R to D1 and D2,

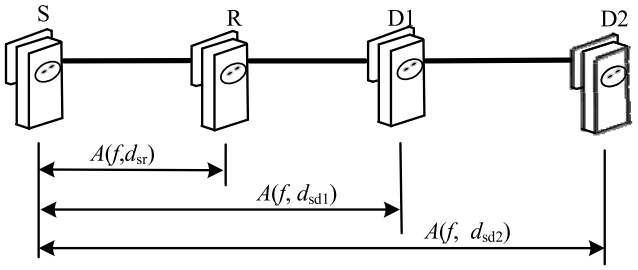

FIGURE 1. The considered system model consisting of four PLC modems: A source S, a relay R, a near-user D1 and far-user D2.

and from S to R are complex valued with amplitudes denoted as $h$sd1, $h$sd2, $h$rd1, $h$rd2 and $h$sr, respectively, with corresponding distances $d$sd1, $d$sd2, $d$rd1, $d$rd2, and $d$sr. The amplitudes of all channel fading coefficients are assumed to be log-normal distributed, the PDF of which is given by

$$f(h_i) = \frac{\zeta}{\sqrt{2\pi}\sigma_i h_i} \exp\left(-\frac{(\zeta \ln(h_i) - \mu_i)^2}{2\sigma_i^2}\right), \quad (1)$$

where $i \in \{\text{sr}, \text{sd1}, \text{sd2}, \text{rd1}, \text{rd2}, \zeta = 10/\ln(10), \mu i$ and σi are the mean and standard deviation of $10\log(hi)$, respectively. It should be noted that the log-normal model adopted here takes into account the random effects introduced by branches and mismatched loads presented in the ensemble of network topologies. In addition, the frequency/distance dependent attenuation is incorporated into our system model and is denoted by $A(f, d_i) = \exp(-(b_0 + b_1 f^m)d_i)$, where b_0 and b_1 are constants determined from measurements, m is the exponent of the attenuation factor, and f is the operating frequency.

The data transmission of each time block consists of two consecutive equal length phases. During the first phase, S broadcasts the superimposed signal by linearly combing the symbol $x_1^{(1)}$ for D1 and the symbol $x_2^{(1)}$ for D2 to R and D1. After receiving the superimposed signal, D1 and R try to decode $x_1^{(1)}$ by treating $x_2^{(1)}$ as interference. If R correctly decodes $x_1^{(1)}$, it will cancel $x_1^{(1)}$ from its received mixed signal and then further decode $x_2^{(1)}$ by applying successive interference cancellation (SIC) technique; otherwise, R will fail to decode $x_1^{(1)}$ and $x_2^{(1)}$ We note that the decoding operations at R and D1 are independent due to the channel fading is independent across different links. If $x_2^{(1)}$ is decoded correctly, R will further forward it to D2 during the second phase and then D2 will try to decode $x_2^{(1)}$ after hearing it from R; otherwise, both R and D2 keep silent during the second phase.

Meanwhile, during the second phase, D1 and S will take different actions depending on the various decoding status of $x_1^{(1)}$ at D1 in the first phase. For the case that D1 correctly decode $x_1^{(1)}$ in the first phase, it will feed back a 1-bit positive ACK to S. After receiving this feedback, during the second phase, instead of only enabling the transmission of R in the TCN scheme, S is also allowed to participate in data transmission and sends the new data symbol $x_1^{(2)}$ to D1 through the direct link transmission mode. On the other hand, if D1 fails to decode $x_1^{(1)}$ during the first phase, it will feed back a 1-bit NACK to notify S that the cooperative data transmission mode between them should be adopted. We know that D1 can also overhear $x_2^{(1)}$ by listening the signal forwarded by R during the second phase. Hence, upon hearing the NACK, S keeps silent during the second phase and D1 combines its received signals in both phases using the MRC technique to decode $x_2^{(1)}$ by treating $x_1^{(1)}$ as interference. Then, by using SIC technique, D1 will retrieve the desired signal $x_1^{(1)}$ after correctly decoding and perfectly cancelling $x_2^{(1)}$.

A. SIGNAL MODEL OF ACN SCHEME

In the first phase, S broadcasts the superimposed signal $x^{(1)} = \sqrt{a_1^{(1)}P_s}x_1^{(1)} + \sqrt{a_2^{(1)}P_s}x_2^{(1)}$ to R and D1, where P_s denotes the source transmit power, $a_1^{(1)}$ and $a_2^{(1)}$ are power allocation coefficients for $x_1^{(1)}$ and $x_2^{(1)}$, respectively, with $a_1^{(1)} + a_2^{(1)} = 1$. It is assumed that $a_1^{(1)} > a_1^{(2)}$, i.e., $x_1^{(1)}$ is allocated with more power, since the required quality of service (QoS) of D1are given a higher priority [31]. R and D1 try to decode $x_1^{(1)}$ first by treating $x_2^{(1)}$ as interference. By using SIC technique, R further decodes $x_2^{(1)}$ after decoding and cancelling $x_1^{(1)}$. Using the substitution $A_i = A(fd_i)$, the received signals at the R and D1 during the first phase can be given respectively by

$$y_{\text{d1}}^{(1)} = h_{\text{sd1}}A_{\text{sd1}}x^{(1)} + n_{\text{d1}}^{(1)} \quad (2)$$

and

$$y_{\text{r}}^{(1)} = h_{\text{sr}}A_{\text{sr}}x^{(1)} + n_{\text{r}}^{(1)}, \quad (3)$$

where $n_{\text{d1}}^{(1)}$ and $n_{\text{r}}^{(1)}$ respectively represent the noise at R and D1 with variances $(\sigma_{\text{d1}}^{(1)})^2$ and $(\sigma_{\text{r}}^{(1)})^2$. This noise typically consists of background and impulsive noise [29], [30], [32].

Assuming that $x_2^{(1)}$ is decoded successfully during the first phase, R will forward it to D2 with transmit power P_r during the second phase. Thus, the received signal at D2 is given by

$$y_{\text{d2}}^{(2)} = h_{\text{rd2}}A_{\text{rd2}}\sqrt{P_r}x_2^{(1)} + n_{\text{d2}}^{(2)}, \quad (4)$$

where $n_{\text{d2}}^{(2)}$ is the noise at D2 with variance $(\sigma_{\text{d2}}^{(2)})^2$.

It is assumed that $E[|x_1^{(1)}|^2] = E[|x_2^{(1)}|^2] = 1$ and the noise variance at each PLC modem is identical and equals σ^2, i.e., $(\sigma_{\text{d1}}^{(1)})^2 = (\sigma_{\text{r}}^{(1)})^2 = (\sigma_{\text{d2}}^{(2)})^2 = \sigma^2$. Therefore, according to the predefined decoding order of data symbols, the received signal-to-interference-and-noise ratios (SINRs) at R and D1 to decode $x_1^{(1)}$ are respectively given by

$$\gamma_{\text{d1}}^{(1)} = \frac{|h_{\text{sd1}}|^2 A_{\text{sd1}}^2 a_1^{(1)}\rho_s}{|h_{\text{sd1}}|^2 A_{\text{sd1}}^2 a_2^{(1)}\rho_s + 1} \quad (5)$$

and

$$\gamma_{\text{r},1}^{(1)} = \frac{|h_{\text{sr}}|^2 A_{\text{sr}}^2 a_1^{(1)}\rho_s}{|h_{\text{sr}}|^2 A_{\text{sr}}^2 a_2^{(1)}\rho_s + 1}, \quad (6)$$

where $\rho_s = \frac{P_s}{\sigma^2}$ is the source transmit SNR.

The received SNR at R to decode $x_2^{(1)}$ is given by

$$\gamma_{\mathrm{r},2}^{(1)} = |h_{\mathrm{sr}}|^2 A_{\mathrm{sr}}^2 a_2^{(1)} \rho_s. \tag{7}$$

The received SNR at D2 to decode $x_2^{(1)}$ can be given by

$$\gamma_{\mathrm{d2}}^{(2)} = |h_{\mathrm{rd2}}|^2 A_{\mathrm{rd2}}^2 \rho_r. \tag{8}$$

where $\rho_r = \frac{P_r}{\sigma^2}$ is the relay transmit SNR.

Moreover, the received signal at D1 during the second phase depends on the adopted data transmission mode.

1) DIRECT DATA TRANSMISSION MODE

In this case, S transmits the new data symbol $x_1^{(2)}$ to D1 with transmit power $a_1^{(2)} P_s$. Besides, D1 can also overhear the signal forwarded by R, thus the received signal at D1 is given by

$$y_{\mathrm{d1}}^{(2)} = h_{\mathrm{sd1}} A_{\mathrm{sd1}} \sqrt{a_1^{(2)} P_s} x_1^{(2)} + h_{\mathrm{rd1}} A_{\mathrm{rd1}} \sqrt{P_r} x_2^{(1)} + n_{\mathrm{d1}}^{(2)}, \tag{9}$$

where $n_{\mathrm{d1}}^{(2)}$ is the noise at D1 with variance $(\sigma_{\mathrm{d1}}^{(2))})^2$. With the assumption that $(\sigma_{\mathrm{d1}}^{(2)})^2 = \sigma^2$, the received SINR at D1 to decode $x_1^{(2)}$ can be expressed as

$$\gamma_{\mathrm{d1}}^{(2)} = \frac{|h_{\mathrm{sd1}}|^2 A_{\mathrm{sd1}}^2 a_1^{(2)} \rho_s}{|h_{\mathrm{rd1}}|^2 A_{\mathrm{rd1}}^2 \rho_r + 1}. \tag{10}$$

2) COOPERATIVE DATA TRANSMISSION MODE

In this case, S keeps silent during the second phase, D1 can only overhear the signal from R, and thus the received signal at D1 in the second phase is given by

$$y_{\mathrm{d1}}^{(2)} = h_{\mathrm{rd1}} A_{\mathrm{rd1}} \sqrt{P_r} x_2^{(1)} + n_{\mathrm{d1}}^{(2)}. \tag{11}$$

D1 combines it with the signal received in the first phase by using MRC and tries to decode and cancel $\mathrm{x}_2^{(1)}$ to further retrieve its desired signal $\mathrm{x}_1^{(1)}$. Hence, the received SINR and SNR at D1 to decode $\mathrm{x}_2^{(1)}$ and $\mathrm{x}_1^{(1)}$ can be respectively given by

$$\gamma_{\mathrm{d1},2}^{(2)} = \frac{|h_{\mathrm{sd1}}|^2 A_{\mathrm{sd1}}^2 a_2^{(1)} \rho_s}{|h_{\mathrm{sd1}}|^2 A_{\mathrm{sd1}}^2 a_1^{(1)} \rho_s + 1} + |h_{\mathrm{rd1}}|^2 A_{\mathrm{rd1}}^2 \rho_r, \tag{12}$$

and

$$\gamma_{\mathrm{d1},1}^{(2)} = |h_{\mathrm{sd1}}|^2 A_{\mathrm{sd1}}^2 a_1^{(1)} \rho_s. \tag{13}$$

B. SIGNAL MODEL OF BANCHMARK SCHEMES

In our proposed scheme, the power consumption of S is respectively given as P_s for the direct transmission mode and $(1+a_1^{(2)})P_s$ for the cooperative transmission mode, while the power consumption of R in a normalized time block equals Pr. Thus, the overall power consumption of our scheme in each normalized time block is at most $\frac{1}{2}(1+a_1^{(2)})P_s + \frac{1}{2}P_r$.

The TDMA scheme is chosen as a representative scheme of OMA in this paper to compare the system performance between OMA and the proposed NOMA scheme, which is consistent with [19], [20], and [23]. For the benchmark TDMA scheme consisting of three phases with equal length, we set the transmit power of S during the first two phases as $(\frac{3}{4} + \frac{3}{2}a_1^{(2)})P_s$ and $\frac{3}{4}P_s$, respectively, and the transmit power of R in the last phase as $\frac{3}{2}P_r$. In this way, the overall power consumption of the TDMA scheme in a normalized time block is equal to the maximum power consumption of the proposed ACN scheme, which facilitates a relatively fair comparison between this two schemes. During the first phase, S sends $x_1^{(1)}$to D1 with transmit power $(\frac{3}{4} + \frac{3}{2}a_1^{(2)})P_s$. The received signal at D1 can be given by

$$y_{\mathrm{d1}}^{\mathrm{TDMA}} = h_{\mathrm{sd1}} A_{\mathrm{sd1}} \sqrt{\left(\frac{3}{4} + \frac{3}{2}a_1^{(2)}\right) P_s} x_1^{(1)} + n_{\mathrm{d1}}^{(1)}. \tag{14}$$

The corresponding received SNR at D1 to decode $x_1^{(1)}$ is given by

$$\gamma_{\mathrm{d1}}^{\mathrm{TDMA}} = \left(\frac{3}{4} + \frac{3}{2}a_1^{(2)}\right) |h_{\mathrm{sd1}}|^2 A_{\mathrm{sd1}}^2 \rho_s. \tag{15}$$

During the second phase, S sends $x_2^{(1)}$ to R with transmit power $\frac{3}{4}P_s$. The received signal at R can be expressed as

$$y_{\mathrm{r}}^{\mathrm{TDMA}} = h_{\mathrm{sr}} A_{\mathrm{sr}} \sqrt{\frac{3}{4} P_s} x_2^{(1)} + n_{\mathrm{r}}^{(1)}. \tag{16}$$

The received SNR at R to decode $x_2^{(1)}$ can be given by

$$\gamma_{\mathrm{r}}^{\mathrm{TDMA}} = \frac{3}{4} |h_{\mathrm{sr}}|^2 A_{\mathrm{sr}}^2 \rho_s. \tag{17}$$

In the last phase, R forwards $x_2^{(1)}$ to D2 with transmit power $\frac{3}{2}P_r$. The received signal at D2 is given by

$$y_{\mathrm{d2}}^{\mathrm{TDMA}} = h_{\mathrm{rd2}} A_{\mathrm{rd2}} \sqrt{\frac{3}{2} P_r} x_2^{(1)} + n_{\mathrm{d2}}^{(2)}. \tag{18}$$

The received SNR at D2 to decode $x_2^{(1)}$ is given by

$$\gamma_{\mathrm{d2}}^{\mathrm{TDMA}} = \frac{3}{2} |h_{\mathrm{rd2}}|^2 A_{\mathrm{rd2}}^2 \rho_r. \tag{19}$$

Note that for the sake of fairness, $x_1^{(1)}$, $x_2^{(1)}$, $n_{\mathrm{d1}}^{(1)}$, $n_{\mathrm{r}}^{(1)}$ and $n_{\mathrm{d2}}^{(2)}$ here are the same as the corresponding variables in our scheme.

We now briefly describe another benchmark scheme, i.e., the TCN scheme, due to it is the simplification of our scheme. The TCN scheme is also consists of two equal length phases. In the first phase, S broadcasts the superimposed signal to relay R and D1 with power allocation coefficients $a_1^{(1)}(1+a_1^{(2)})P_s$ for $x_1^{(1)}$ and $a_2^{(1)}(1+a_1^{(2)})P_s$ for $x_2^{(1)}$. D1 decodes $x_1^{(1)}$ while R decodes and cancels $x_1^{(1)}$ from its received signal to further decode $x_2^{(1)}$. Then, during the second phase, R forwards $x_2^{(1)}$ to D2 with transmit powerP_r. S keeps silent no matter whether D1 can correctly decode $x_1^{(1)}$ or not in the first phase. The signal mode of the TCN scheme can be obtained by replacing the source transmit power P_s with $(1+a_1^{(2)})P_s$ in (2)-(8).

III. PERFORMANCE ANALYSIS

In this section, we analyze the achievable performance of the proposed ACN scheme and two benchmark schemes in term of system throughput. It should be pointed out that different from conventional communication networks, PLC channels are subject to both background and impulsive noise, so that the channel capacity and system throughput is calculated depending on the adopted coding/decoding strategy, i.e., erasure decoding and non-erasure decoding. For simplifying the system performance analysis, this paper considers below the erasure coding strategy only, which is line with [19], [20]. Of course, the performance of cooperative NOMA networks will be further enhanced if the non-erasure coding strategy is exploited. However, it is not the concerns of this paper since we focus on the performance enhancement by the improved cooperative NOMA scheme.

Both the target rates of the data symbol $x_1^{(1)}$ and $x_1^{(2)}$ are set as V_1, while the target rate of the data symbol $x_2^{(1)}$ is set as V_2. According to the Shannon coding theorem, if the channel capacity is greater than the signal transmission rate, the successful data transmission can be achieved; otherwise, an outage event occurs and data symbols cannot be decoded correctly by receiver.

A. SYSTEM THROUGHPUT OF ACN SCHEME

For our scheme, let C_1 and C_2 respectively denote the system throughput under the direct transmission mode and the cooperative transmission mode. The system throughput of the proposed ACN scheme is given by

$$C = C_1 + C_2. \tag{20}$$

The event definitions and corresponding decoding results are showed in Table 1, where $R_1 = 2^{2V_1/(1-p)}$ and $R_2 = 2^{2V_2/(1-p)}$ with p representing the occurrence probability of the impulsive noise. Note that the event D occurs only when the direct transmission mode is adopted, while the events E and F occur only when the cooperative transmission mode is adopted.

1) DIRECT DATA TRANSMISSION MODE

In this model, the event A always happen and the system throughput can be calculated as

$$\begin{aligned} C_1 = {} & (2V_1 + V_2)\Pr\{A, B, C, D\} \\ & + (V_1 + V_2)\Pr\left\{A, B, C, \overline{D}\right\} \\ & + 2V_1 \Pr\left\{A, B, \overline{C}, D\right\} + 2V_1 \Pr\left\{A, \overline{B}, D\right\} \\ & + V_1 \Pr\left\{A, B, \overline{C}, \overline{D}\right\} + V_1 \Pr\left\{A, \overline{B}, \overline{D}\right\}, \end{aligned} \tag{21}$$

where $\overline{B}$, $\overline{C}$ and $\overline{D}$ are the complementary event of B, C and D, respectively.

According to the event definition, the events B and C are dependent and the event D is related with the events A and B. However, the throughput analysis can be decoupled because the channel fading is independent over different links. Therefore, (21) can be rewritten as

$$\begin{aligned} C_1 = {} & (2V_1 + V_2)\Pr\{A, D\}\Pr\{B\}\Pr\{C\} \\ & + (V_1 + V_2)\Pr\left\{A, \overline{D}\right\}\Pr\{B\}\Pr\{C\} \\ & + 2V_1 \Pr\{A, D\}\left(1 - \Pr\{B\}\Pr\{C\}\right) \\ & + V_1 \Pr\left\{A, \overline{D}\right\}\left(1 - \Pr\{B\}\Pr\{C\}\right), \end{aligned} \tag{22}$$

where A and D or $\overline{D}$ are related and the system throughput associated with them cannot be decoupled.

TABLE 1. Event definitions and decoding results.

Phase	Event	Definition	Decoding result
First	A	$\gamma_{\mathrm{d1}}^{(1)} \geq R_1$	Correct $x_1^{(1)}$
	B	$\gamma_{\mathrm{r,1}}^{(1)} \geq R_1, \gamma_{\mathrm{r,2}}^{(1)} \geq R_2$	Correct $x_1^{(1)}$ and $x_2^{(1)}$
Second	C	$\gamma_{\mathrm{d2}}^{(2)} \geq R_2$	Correct $x_2^{(1)}$
	D	$\gamma_{\mathrm{d1}}^{(2)} \geq R_1$	Correct $x_1^{(2)}$
	E	$\gamma_{\mathrm{d1,2}}^{(2)} \geq R_2$	Correct $x_2^{(1)}$
	F	$\gamma_{\mathrm{d1,1}}^{(2)} \geq R_1$	Correct $x_1^{(1)}$

The joint probability of the events A and D is calculated as

$$\Pr\{A, D\} = \Pr\left\{\gamma_{\mathrm{d1}}^{(1)} \geq R_1, \gamma_{\mathrm{d1}}^{(2)} \geq R_1\right\}. \tag{23}$$

By substituting (5) and (10) into (23), we obtain

$$\begin{aligned} \Pr\{A, D\} = \Pr\Bigg\{ & \frac{|h_{\mathrm{sd1}}|^2 A_{\mathrm{sd1}}^2 a_1^{(1)} \rho_s}{|h_{\mathrm{sd1}}|^2 A_{\mathrm{sd1}}^2 a_2^{(1)} \rho_s + 1} \geq R_1, \\ & \frac{|h_{\mathrm{sd1}}|^2 A_{\mathrm{sd1}}^2 a_1^{(2)} \rho_s}{|h_{\mathrm{rd1}}|^2 A_{\mathrm{rd1}}^2 \rho_r + 1} \geq R_1 \Bigg\}. \end{aligned} \tag{24}$$

According to the properties of log-normal distributed variable, the variable $|h_i|^2$ follows log-normal distribution with parameter $|h_i|^2 \sim \ln n\left(2\mu_i, (2\sigma_i)^2\right)$. The PDF, CDF and CCDF of the variable $|h_i|^2$ can be respectively expressed as

$$f_{|h_i|^2}(z) = \frac{\zeta}{\sqrt{8\pi}\sigma_i z} \exp\left(-\frac{(\zeta \ln(z) - 2\mu_i)^2}{8\sigma_i^2}\right), \tag{25}$$

$$F_{|h_i|^2}(z) = 1 - Q\left(\frac{\zeta \ln(z) - 2\mu_i}{2\sigma_i}\right), \tag{26}$$

and

$$\overline{F}_{|h_i|^2}(z) = Q\left(\frac{\zeta \ln(z) - 2\mu_i}{2\sigma_i}\right), \tag{27}$$

where $Q(\cdot)$ is the Q-function, which is defined as

$$Q(z) = \frac{1}{\sqrt{2\pi}} \int_z^{\infty} \exp\left(-\frac{t^2}{2}\right) \mathrm{d}t. \tag{28}$$

Hence, using (25)-(27), along with some basic mathematical manipulations, we can get the result of $\Pr\{A, D\}$ as **Lemma 1.**

Lemma 1: Let the variables $\beta_0 = \frac{R_1}{A_{\mathrm{sd1}}^2\left(a_1^{(1)} - a_2^{(1)} R_1\right)\rho_s}$, $\beta_1 = \frac{R_1}{A_{\mathrm{sd1}}^2 a_1^{(2)} \rho_s}$ *and* $\Phi\left(|h_{\mathrm{sd1}}|^2\right) = \frac{|h_{\mathrm{sd1}}|^2 A_{\mathrm{sd1}}^2 a_1^{(2)} \rho_s - R_1}{A_{\mathrm{rd1}}^2 \rho_r R_1}$. *The joint*

probability $\Pr\{A, D\}$ *can be expressed as*

$$\Pr\{A, D\} = 1_{\Im_0}\left\{\int_{I_0} \frac{\zeta}{\sqrt{8\pi}\sigma_{\mathrm{sd1}}x}\exp\left(-\frac{(\zeta\ln(x)-2\mu_{\mathrm{sd1}})^2}{8\sigma_{\mathrm{sd1}}^2}\right) \times\left(1-Q\left(\frac{\zeta\ln(\Phi(x))-2\mu_{\mathrm{rd1}}}{2\sigma_{\mathrm{rd1}}}\right)\right)\mathrm{d}x\right\}, \quad (29)$$

where the integral interval $I_0 = \left(\max\left(\beta_0, \beta_1\right), \infty\right)$. *The indicator variable* $1_{\Im_0}$ *equals 1 if the condition* $\Im_0 : a_1^{(1)} > \frac{R_1}{R_1+1}$ *is satisfied; otherwise it equals 0.*

Proof: See the Appendix A.

Following the derivation procedure of $\Pr\{A, D\}$, we derive the joint probability of the events A and $\overline{D}$ as

$$\Pr\left\{A, \overline{D}\right\} = \Pr\left\{\frac{|h_{\mathrm{sd1}}|^2 A_{\mathrm{sd1}}^2 a_1^{(1)}\rho_s}{|h_{\mathrm{sd1}}|^2 A_{\mathrm{sd1}}^2 a_2^{(1)}\rho_s+1} \geq R_1, \frac{|h_{\mathrm{sd1}}|^2 A_{\mathrm{sd1}}^2 a_1^{(2)}\rho_s}{|h_{\mathrm{rd1}}|^2 A_{\mathrm{rd1}}^2\rho_r+1} < R_1\right\}, \quad (30)$$

and the result of $\Pr\left\{A, \overline{D}\right\}$is given in **Lemma 2.**

Lemma 2: The joint probability $\Pr\left\{A, \overline{D}\right\}$ *is derived as* $\Pr\left\{A, \overline{D}\right\} = \phi_{11} + \phi_{12}$. *The two terms respectively equal*

$$\phi_{11} = 1_{\Im_0}\left\{\int_{I_0} \frac{\zeta}{\sqrt{8\pi}\sigma_{\mathrm{sd1}}x}\exp\left(-\frac{(\zeta\ln(x)-2\mu_{\mathrm{sd1}})^2}{8\sigma_{\mathrm{sd1}}^2}\right) \times Q\left(\frac{\zeta\ln(\Phi(x))-2\mu_{\mathrm{rd1}}}{2\sigma_{\mathrm{rd1}}}\right)\mathrm{d}x\right\}, \quad (31)$$

and

$$\phi_{12} = 1_{\Im_1}\left\{Q\left(\frac{\zeta\ln(\beta_0)-2\mu_{\mathrm{sd1}}}{2\sigma_{\mathrm{sd1}}}\right) - Q\left(\frac{\zeta\ln(\beta_1)-2\mu_{\mathrm{sd1}}}{2\sigma_{\mathrm{sd1}}}\right)\right\}, \quad (32)$$

where $1_{\Im_1}$ *is an indicator variable, which equals* 1 *when the condition* $\Im_1 : a_1^{(1)} > \frac{R_1}{R_1+1}$, $\beta_1 > \beta_0$ *is satisfied. The integral interval* $I_1 = (\beta_0, \beta_1)$.

Proof: See the Appendix A.

By adding (31) and (32) together, the result of $\Pr\left\{A, \overline{D}\right\}$ can be finally obtained.

Furthermore, using the event definition of B along with some mathematical manipulations, the occurrence probability $\Pr\{B\}$ can be derived as

$$\Pr\{B\} = \Pr\left\{\gamma_{\mathrm{r},1}^{(1)} \geq R_1, \gamma_{\mathrm{r},2}^{(1)} \geq R_2\right\} = Q\left(\frac{\zeta\ln(\chi)-2\mu_{\mathrm{sr}}}{2\sigma_{\mathrm{sr}}}\right), \quad (33)$$

when the condition $a_1^{(1)} > \frac{R_1}{R_1+1}$ is satisfied, where the term $\chi = \max\left(\frac{R_1}{A_{\mathrm{sr}}^2\left(a_1^{(1)}-a_2^{(1)}R_1\right)\rho_s}, \frac{R_2}{A_{\mathrm{sr}}^2 a_2^{(1)}\rho_s}\right)$. Similarly, the occurrence probability $\Pr\{C\}$ is derived as

$$\Pr\{C\} = \Pr\left\{\gamma_{\mathrm{d2}}^{(2)} \geq R_2\right\} = Q\left(\frac{\zeta\ln(\eta)-2\mu_{\mathrm{rd2}}}{2\sigma_{\mathrm{rd2}}}\right), \quad (34)$$

where the term $\eta = \frac{R_2}{A_{\mathrm{rd2}}^2\rho_r}$.

By substituting the results of $\Pr\{A, D\}$, $\Pr\left\{A, \overline{D}\right\}$, $\Pr\{B\}$ and $\Pr\{C\}$ into (22), the system throughput in the direct data transmission mode can be finally obtained.

2) COOPERATIVE DATA TRANSMISSION MODE

Under this data transmission mode, instead of the event A, its complementary event $\overline{A}$ always occurs, that is, D1 can never successfully decode its desire signal by only overhearing the S during the first phase. Therefore, the system throughput associated with the cooperative transmission mode can be calculated as

$$\begin{aligned} C_2 = {} & (V_1+V_2)\Pr\left\{\overline{A}, E, F\right\}\Pr\{B\}\Pr\{C\} \\ & + V_2\left(\Pr\left\{\overline{A}, E, \overline{F}\right\} + \Pr\left\{\overline{A}, \overline{E}\right\}\right)\Pr\{B\}\Pr\{C\} \\ & + V_1\Pr\left\{\overline{A}, E, F\right\}(1-\Pr\{B\}\Pr\{C\}), \end{aligned} \quad (35)$$

where $\overline{E}$ and $\overline{F}$ are the complementary event of E and F, respectively.

The occurrence probabilities $\Pr\{B\}$ and $\Pr\{C\}$ are not affected by the adopted data transmission mode. As such, we only show the joint probabilities $\Pr\left\{\overline{A}, E, F\right\}$, $\Pr\left\{\overline{A}, E, \overline{F}\right\}$ and $\Pr\left\{\overline{A}, \overline{E}\right\}$ in this part.

The joint probability $\Pr\left\{\overline{A}, E, F\right\}$ can be expressed as

$$\Pr\left\{\overline{A}, E, F\right\} = \Pr\left\{\gamma_{\mathrm{d1}} < R_1, \gamma_{\mathrm{d1},2} \geq R_2, \gamma_{\mathrm{d1},1} \geq R_1\right\}. \quad (36)$$

By substituting (5), (12) and (13) into (36), we can get

$$\Pr\left\{\overline{A}, E, F\right\} = \Pr\left\{\frac{|h_{\mathrm{sd1}}|^2 A_{\mathrm{sd1}}^2 a_1^{(1)}\rho_s}{|h_{\mathrm{sd1}}|^2 A_{\mathrm{sd1}}^2 a_2^{(1)}\rho_s+1} < R_1, |h_{\mathrm{rd1}}|^2 \geq \frac{R_2-\Gamma\left(|h_{\mathrm{sd1}}|^2\right)}{A_{\mathrm{rd1}}^2\rho_r}, |h_{\mathrm{sd1}}|^2 \geq \frac{R_1}{A_{\mathrm{sd1}}^2 a_1^{(1)}\rho_s}\right\}, \quad (37)$$

where $\Gamma\left(|h_{\mathrm{sd1}}|^2\right) = \frac{|h_{\mathrm{sd1}}|^2 A_{\mathrm{sd1}}^2 a_2^{(1)}\rho_s}{|h_{\mathrm{sd1}}|^2 A_{\mathrm{sd1}}^2 a_1^{(1)}\rho_s+1}$.

Lemma 3: The expression of $\Pr\left\{\overline{A}, E, F\right\}$ *can be divided into three parts and equals* $\phi_{21}+\phi_{22}+\phi_{23}$. *In this expression, we set* $\Omega\left(|h_{\mathrm{sd1}}|^2\right) = \frac{R_2-\Gamma\left(|h_{\mathrm{sd1}}|^2\right)}{A_{\mathrm{rd1}}^2 P_r}$, $\beta_2 = \frac{R_2}{A_{\mathrm{sd1}}^2\left(a_2^{(1)}-a_1^{(1)}R_2\right)\rho_s}$, *and* $\beta_3 = \frac{R_1}{A_{\mathrm{sd1}}^2 a_1^{(1)}\rho_s}$. *The first term is*

$$\phi_{21} = 1_{\Im_2}\left\{\int_{I_2} \frac{\zeta}{\sqrt{8\pi}\sigma_{\mathrm{sd1}}x}\exp\left(-\frac{(\zeta\ln(x)-2\mu_{\mathrm{sd1}})^2}{8\sigma_{\mathrm{sd1}}^2}\right) \times Q\left(\frac{\zeta\ln(\Omega(x))-2\mu_{\mathrm{rd1}}}{2\sigma_{\mathrm{rd1}}}\right)\mathrm{d}x\right\}, \quad (38)$$

where the integral interval $I_2 = (\beta_3, \min(\beta_0, \beta_2))$. *The indicator variable* $1_{\Im_2}$ *equals* 1 *when the condition* $\Im_2 : \frac{R_1}{R_1+1} < a_1^{(1)} < \frac{1}{R_2+1}$, $\beta_3 < \min(\beta_0, \beta_2)$ *is satisfied, while it equals* 0 *when this condition cannot be satisfied.*

The second term is

$$\phi_{22} = 1_{\Im_3}\left\{\int_{I_3}\frac{\zeta}{\sqrt{8\pi}\sigma_{\mathrm{sd1}}x}\exp\left(-\frac{(\zeta\ln(x)-2\mu_{\mathrm{sd1}})^2}{8\sigma_{\mathrm{sd1}}^2}\right)\times Q\left(\frac{\zeta\ln(\Omega(x))-2\mu_{\mathrm{rd1}}}{2\sigma_{\mathrm{rd1}}}\right)\mathrm{d}x\right\}, \quad (39)$$

where $I_3 = (\beta_3, \beta_0)$ *is the integral interval and the indicator variable* $1_{\Im_3}$ *equals* 1 *when the condition* $\Im_3 : \max\left(\frac{R_1}{R_1+1}, \frac{1}{R_2+1}\right) < a_1^{(1)}, \beta_3 < \beta_0$ *is satisfied. The last term is*

$$\phi_{23} = 1_{\Im_4}\left\{Q\left(\frac{\zeta\ln(\max(\beta_2,\beta_3))-2\mu_{\mathrm{sd1}}}{2\sigma_{\mathrm{sd1}}}\right) - Q\left(\frac{\zeta\ln(\beta_0)-2\mu_{\mathrm{sd1}}}{2\sigma_{\mathrm{sd1}}}\right)\right\}, \quad (40)$$

where the indicator variable $1_{\Im_4}$ *equals 1 when the condition* $\Im_4 : \frac{R_1}{R_1+1} < a_1^{(1)} < \frac{1}{R_2+1}, \max(\beta_2,\beta_3) < \beta_0$ *is satisfied, while it equals* 0 *when this condition cannot be satisfied.*

Proof: See the Appendix B.

The result of $\Pr\left\{\overline{A}, E, F\right\}$ can be finally achieved by adding (38), (39) and (40) together.

Following the same procedure, we can also derive the joint probability associated with the event $\overline{A}$, E and $\overline{F}$. The expression of $\Pr\left\{\overline{A}, E, \overline{F}\right\}$ can be written as

$$\Pr\left\{\overline{A}, E, \overline{F}\right\} = \Pr\left\{\frac{|h_{\mathrm{sd1}}|^2 A_{\mathrm{sd1}}^2 a_1^{(1)}\rho_s}{|h_{\mathrm{sd1}}|^2 A_{\mathrm{sd1}}^2 a_2^{(1)}\rho_s + 1} < R_1\,, \; |h_{\mathrm{rd1}}|^2 \geq \frac{R_2 - \Gamma\left(|h_{\mathrm{sd1}}|^2\right)}{A_{\mathrm{rd1}}^2\rho_r}, \; |h_{\mathrm{sd1}}|^2 < \frac{R_1}{A_{\mathrm{sd1}}^2 a_1^{(1)}\rho_s}\right\}. \quad (41)$$

Lemma 4: The expression of $\Pr\left\{\overline{A}, E, \overline{F}\right\}$ *consists of three parts, i.e.,* $\Pr\left\{\overline{A}, E, \overline{F}\right\} = \phi_{31} + \phi_{32} + \phi_{33}$. *The first term is*

$$\phi_{31} = 1_{\Im_5}\left\{\int_{I_5}\frac{\zeta}{\sqrt{8\pi}\sigma_{\mathrm{sd1}}x}\exp\left(-\frac{(\zeta\ln(x)-2\mu_{\mathrm{sd1}})^2}{8\sigma_{\mathrm{sd1}}^2}\right)\times Q\left(\frac{\zeta\ln(\Omega(x))-2\mu_{\mathrm{rd1}}}{2\sigma_{\mathrm{rd1}}}\right)\mathrm{d}x\right\}, \quad (42)$$

where the integral interval $I_5 = (0, \min(\beta_0, \beta_2, \beta_3))$. *The indicator variable* $1_{\Im_5}$ *equals* 1 *when the condition* $\Im_5 : \frac{R_1}{R_1+1} < a_1^{(1)} < \frac{1}{R_2+1}$ *is satisfied; otherwise, it equals* 0. *The second term is*

$$\phi_{32} = 1_{\Im_6}\left\{\int_{I_6}\frac{\zeta}{\sqrt{8\pi}\sigma_{\mathrm{sd1}}x}\exp\left(-\frac{(\zeta\ln(x)-2\mu_{\mathrm{sd1}})^2}{8\sigma_{\mathrm{sd1}}^2}\right)\times Q\left(\frac{\zeta\ln(\Omega(x))-2\mu_{\mathrm{rd1}}}{2\sigma_{\mathrm{rd1}}}\right)\mathrm{d}x\right\}, \quad (43)$$

where the integral interval $I_6 = (0, \min(\beta_0, \beta_3))$ *and the indicator variable* $1_{\Im_5}$ *equals* 1 *when the condition* $\Im_6 : \max\left(\frac{R_1}{R_1+1}, \frac{1}{R_2+1}\right) < a_1^{(1)}$ *is satisfied. The third term is*

$$\phi_{33} = 1_{\Im_7}\left\{Q\left(\frac{\zeta\ln(\beta_2)-2\mu_{\mathrm{sd1}}}{2\sigma_{\mathrm{sd1}}}\right) - Q\left(\frac{\zeta\ln(\min(\beta_0,\beta_3))-2\mu_{\mathrm{sd1}}}{2\sigma_{\mathrm{sd1}}}\right)\right\}, \quad (44)$$

where the indicator variable $1_{\Im_7}$ *equals* 1 *when the condition* $\Im_7 : \frac{R_1}{R_1+1} < a_1^{(1)} < \frac{1}{R_2+1}, \beta_2 < \min(\beta_0, \beta_3)$ *is satisfied, while it equals 0 if this condition cannot be satisfied.*

Proof: See the Appendix B.

The result of $\Pr\left\{\overline{A}, E, \overline{F}\right\}$ can be finally obtained by adding (42), (43) and (44) together.

Similarly, we now derive the expression of $\Pr\left\{\overline{A}, \overline{E}\right\}$. According its definition, we get

$$\Pr\left\{\overline{A}, \overline{E}\right\} = \Pr\left\{\frac{|h_{\mathrm{sd1}}|^2 A_{\mathrm{sd1}}^2 a_1^{(1)}\rho_s}{|h_{\mathrm{sd1}}|^2 A_{\mathrm{sd1}}^2 a_2^{(1)}\rho_s + 1} < R_1\,, \; h_{\mathrm{rd1}}^2 < \frac{R_2 - \Gamma\left(|h_{\mathrm{sd1}}|^2\right)}{A_{\mathrm{rd1}}^2\rho_r}\right\}. \quad (45)$$

Lemma 5: The expression of $\Pr\left\{\overline{A}, \overline{E}\right\}$ *consists of two parts and equals* $\phi_{41} + \phi_{42}$. *The two terms are*

$$\phi_{41} = 1_{\Im_8}\left\{\int_{I_8}\frac{\zeta}{\sqrt{8\pi}\sigma_{\mathrm{sd1}}x}\exp\left(-\frac{(\zeta\ln(x)-2\mu_{\mathrm{sd1}})^2}{8\sigma_{\mathrm{sd1}}^2}\right)\times\left(1 - Q\left(\frac{\zeta\ln(\Omega(x))-2\mu_{\mathrm{rd1}}}{2\sigma_{\mathrm{rd1}}}\right)\right)\mathrm{d}x\right\}, \quad (46)$$

and

$$\phi_{42} = 1_{\Im_9}\left\{\int_{I_9}\frac{\zeta}{\sqrt{8\pi}\sigma_{\mathrm{sd1}}x}\exp\left(-\frac{(\zeta\ln(x)-2\mu_{\mathrm{sd1}})^2}{8\sigma_{\mathrm{sd1}}^2}\right)\times\left(1 - Q\left(\frac{\zeta\ln(\Omega(x))-2\mu_{\mathrm{rd1}}}{2\sigma_{\mathrm{rd1}}}\right)\right)\mathrm{d}x\right\}, \quad (47)$$

where the indicator variable $1_{\Im_8}$ *equals* 1 *when the condition* $\Im_8 : \frac{R_1}{R_1+1} < a_1^{(1)} < \frac{1}{R_2+1}$ *is satisfied and* $1_{\Im_9}$ *equals* 1 *when the condition* $\Im_9 : \max\left(\frac{R_1}{R_1+1}, \frac{1}{R_2+1}\right) < a_1^{(1)}$ *is satisfied. The integral intervals* I_8 *and* I_9 *equal* $(0, \min(\beta_0, \beta_2))$ *and* $(0, \beta_0)$, *respectively.*

Proof: See the Appendix B.

The result of $\Pr\left\{\overline{A}, \overline{E}\right\}$ can be achieved by adding (46) and (47) together. By substituting the results of $\Pr\left\{\overline{A}, E, F\right\}$, $\Pr\left\{\overline{A}, E, \overline{F}\right\}$ and $\Pr\left\{\overline{A}, \overline{E}\right\}$ into (35), we finally obtain the system throughput of the proposed ACN scheme under the cooperative data transmission mode.

Remark 1: From the derived expressions of our ACN scheme, we can see that the system throughput is affected by many system parameters, such as the power allocation coefficients, source and relay transmit powers, occurrence probability of the impulsive noise. A favorable system performance can be supported by well-designed parameters and optimizing these system parameters is crucial to maximize the system performance. However, it is challenging to obtain expression for the joint optimal parameters. Therefore, we conduct

extensive computer simulations in simulation results section to find the optimal values of these parameters that will offer the maximum system throughput.

B. SYSTEM THROUGHPUT OF TDMA SCHEME

Based on the signal model described in Section III, the system throughput of the TDMA scheme can be expressed as

$$\begin{aligned} C^{\mathrm{TDMA}} &= (V_1+V_2)\Pr\left\{\gamma_{\mathrm{d1}}^{\mathrm{TDMA}} \geq R_3\right\}\Pr\left\{\gamma_{\mathrm{r}}^{\mathrm{TDMA}} \geq R_4\right\} \\ &\quad \times \Pr\left\{\gamma_{\mathrm{d2}}^{\mathrm{TDMA}} \geq R_4\right\} + V_1 \Pr\left\{\gamma_{\mathrm{d1}}^{\mathrm{TDMA}} \geq R_3\right\} \\ &\quad \times \left(1-\Pr\left\{\gamma_{\mathrm{r}}^{\mathrm{TDMA}} \geq R_4\right\}\Pr\left\{\gamma_{\mathrm{d2}}^{\mathrm{TDMA}} \geq R_4\right\}\right) \\ &\quad + V_2\left(1-\Pr\left\{\gamma_{\mathrm{d1}}^{\mathrm{TDMA}} \geq R_3\right\}\right)\Pr\left\{\gamma_{\mathrm{r}}^{\mathrm{TDMA}} \geq R_4\right\} \\ &\quad \times \Pr\left\{\gamma_{\mathrm{d2}}^{\mathrm{TDMA}} \geq R_4\right\}, \end{aligned} \tag{48}$$

where $R_3 = 2^{3V_1/((1-p))}$, $R_4 = 2^{3V_2/(1-p)}$.

Using (15) and using (27), we can get the occurrence probability $\Pr\left\{\gamma_{\mathrm{d1}}^{\mathrm{TDMA}} \geq R_3\right\}$ as

$$\begin{aligned} \Pr\left\{\gamma_{\mathrm{d1}}^{\mathrm{TDMA}} \geq R_3\right\} &= \Pr\left\{|h_{\mathrm{sd1}}|^2 \geq \frac{R_3}{A_{\mathrm{sd1}}^2\left(\frac{3}{4}+\frac{3}{2}a_1^{(2)}\right)\rho_s}\right\} \\ &= Q\left(\frac{\zeta \ln\left(\Xi_{\mathrm{sd1}}\right) - 2\mu_{\mathrm{sd1}}}{2\sigma_{\mathrm{sd1}}}\right), \end{aligned} \tag{49}$$

where the term $\Xi_{\mathrm{sd1}} = \frac{R_3}{A_{\mathrm{sd1}}^2\left(\frac{3}{4}+\frac{3}{2}a_1^{(2)}\right)P_s}$.

Similarly, we derive the occurrence probabilities $\Pr\left\{\gamma_{\mathrm{r}}^{\mathrm{TDMA}} \geq R_4\right\}$ and $\Pr\left\{\gamma_{\mathrm{d2}}^{\mathrm{TDMA}} \geq R_4\right\}$ as

$$\begin{aligned} \Pr\left\{\gamma_{\mathrm{r}}^{\mathrm{TDMA}} \geq R_4\right\} &= \Pr\left\{|h_{\mathrm{sr}}|^2 \geq \frac{4R_4}{3A_{\mathrm{sr}}^2\rho_s}\right\} \\ &= Q\left(\frac{\zeta \ln\left(\Xi_{\mathrm{sr}}\right) - 2\mu_{\mathrm{sr}}}{2\sigma_{\mathrm{sr}}}\right), \end{aligned} \tag{50}$$

and

$$\begin{aligned} \Pr\left\{\gamma_{\mathrm{d2}}^{\mathrm{TDMA}} \geq R_4\right\} &= \Pr\left\{|h_{\mathrm{rd2}}|^2 \geq \frac{2R_4}{3A_{\mathrm{rd2}}^2\rho_r}\right\} \\ &= Q\left(\frac{\zeta \ln\left(\Xi_{\mathrm{rd2}}\right) - 2\mu_{\mathrm{rd2}}}{2\sigma_{\mathrm{rd2}}}\right), \end{aligned} \tag{51}$$

respectively, where the terms $\Xi_{\mathrm{sr}} = \frac{4R_4}{3A_{\mathrm{sr}}^2\rho_s}$ and $\Xi_{\mathrm{rd2}} = \frac{2R_4}{3A_{\mathrm{rd2}}^2\rho_r}$.

The system throughput of the TDMA scheme can be finally obtained by substituting (49)-(51) into (48).

Remark 2: Note that here the derived throughput (48) *consists of three parts, which represents various decoding status at D1, R and D2. The first two parts corresponds to the throughput* (21) *of the proposed scheme under the direct data transmission mode, while the last part corresponds to the throughput* (35) *of the proposed scheme under the cooperative data transmission mode. Comparing this two schemes, it is obvious that there exists more events and subcases in our scheme, such as the events D, E, F and the associated subcases. In TDMA scheme, S never participate in the second phase's data transmission even if the link quality from S to R is pretty good, which results in an inefficient system throughput. Meanwhile, there does not exist any chances to retrieve* $x_1^{(1)}$ *for D1 when it fails in decoding this desired signal in the first phase, which degrades the reception reliability of* $x_1^{(1)}$ *at D1. In this sense, the system performance of the TDMA scheme is inferior to that of our scheme.*

C. SYSTEM THROUGHPUT OF TCN SCHEME

We derive the system throughput of the benchmark TCN scheme as

$$\begin{aligned} &C^{\mathrm{TCN}} \\ &= (V_1+V_2)\Pr\left\{\gamma_{\mathrm{d1}}^{\mathrm{TCN}} \geq R_1\right\} \\ &\quad \times \Pr\left\{\gamma_{\mathrm{r},1}^{\mathrm{TCN}} \geq R_1, \gamma_{\mathrm{r},2}^{\mathrm{TCN}} \geq R_2\right\} \times \Pr\left\{\gamma_{\mathrm{d2}}^{\mathrm{TCN}} \geq R_2\right\} \\ &\quad + V_1 \Pr\left\{\gamma_{\mathrm{d1}}^{\mathrm{TCN}} \geq R_1\right\}\left(1-\Pr\left\{\gamma_{\mathrm{r},1}^{\mathrm{TCN}} \geq R_1, \gamma_{\mathrm{r},2}^{\mathrm{TCN}} \geq R_2\right\}\right. \\ &\quad \left.\times \Pr\left\{\gamma_{\mathrm{d2}}^{\mathrm{TCN}} \geq R_2\right\}\right) + V_2\left(1-\Pr\left\{\gamma_{\mathrm{d1}}^{\mathrm{TCN}} \geq R_1\right\}\right) \\ &\quad \times \Pr\left\{\gamma_{\mathrm{r},1}^{\mathrm{TCN}} \geq R_1, \gamma_{\mathrm{r},2}^{\mathrm{TCN}} \geq R_2\right\}\Pr\left\{\gamma_{\mathrm{d2}}^{\mathrm{TCN}} \geq R_2\right\}, \end{aligned} \tag{52}$$

where the terms $\gamma_{\mathrm{d1}}^{\mathrm{TCN}}$, $\gamma_{\mathrm{r},1}^{\mathrm{TCN}}$, $\gamma_{\mathrm{r},2}^{\mathrm{TCN}}$, and $\gamma_{\mathrm{d2}}^{\mathrm{TCN}}$ can be derived by replacing the source transmit power Ps with $\left(1+a_1^{(2)}\right)P$s in (5)-(8).

The events $\gamma_{\mathrm{d1}}^{\mathrm{TCN}} \geq R_1$, $\gamma_{\mathrm{r},1}^{\mathrm{TCN}} \geq R_1$, $\gamma_{\mathrm{r},2}^{\mathrm{TCN}} \geq R_2$ and $\gamma_{\mathrm{d2}}^{\mathrm{TCN}} \geq R_2$ are similar with the events A, B and C but with different source transmit power. Hence, we directly provide the occurrence probabilities associated with these events as

$$\Pr\left\{\gamma_{\mathrm{d1}}^{\mathrm{TCN}} \geq R_1\right\} = Q\left(\frac{\zeta \ln\left(\Theta_{\mathrm{sd1}}\right) - 2\mu_{\mathrm{sd1}}}{\sigma_{\mathrm{sd1}}}\right), \tag{53}$$

$$\Pr\left\{\gamma_{\mathrm{r},1}^{\mathrm{TCN}} \geq R_1, \gamma_{\mathrm{r},2}^{\mathrm{TCN}} \geq R_2\right\} = Q\left(\frac{\zeta \ln\left(\Theta_{\mathrm{sr}}\right) - 2\mu_{\mathrm{sr}}}{2\sigma_{\mathrm{sr}}}\right), \tag{54}$$

and

$$\Pr\left\{\gamma_{\mathrm{d2}}^{\mathrm{TCN}} \geq R_2\right\} = Q\left(\frac{\zeta \ln\left(\Theta_{\mathrm{rd2}}\right) - 2\mu_{\mathrm{rd2}}}{2\sigma_{\mathrm{rd2}}}\right), \tag{55}$$

where $\Theta_{\mathrm{sd1}} = \frac{R_1}{A_{\mathrm{sd1}}^2\left(a_1^{(1)}-a_2^{(1)}R_1\right)\left(1+a_1^{(2)}\right)\rho_s}$, $\Theta_{\mathrm{rd2}} = \frac{R_2}{A_{\mathrm{rd2}}^2\rho_r}$, and

$$\Theta_{\mathrm{sr}} = \max\left(\frac{R_1}{A_{\mathrm{sr}}^2\left(a_1^{(1)}-a_2^{(1)}R_1\right)\left(1+a_1^{(2)}\right)\rho_s}, \frac{R_2}{A_{\mathrm{sr}}^2 a_2^{(1)}\left(1+a_1^{(2)}\right)\rho_s}\right).$$

By substituting (53), (54) and (55) into (52), we can finally get the system throughput of the TCN scheme. W note that the TCN scheme also does not take any measures at S and D1 during the second phase, which is consistent with the TDMA scheme.

TABLE 2. Simulation Parameters.

Parameter	Value
Distance between S and D1, d_{sd1}	120 m
Distance between S and D2, d_{sd2}	200 m
Distance factor, λ	0.4
Target rate $V = V_1 = V_2$	0.8 bits/s/Hz
Source transmit SNR, ρ_s	40 dB
Ratio of transmit power, κ	0.02
Power allocation coefficient, $a_1^{(1)}$	0.85
Power allocation coefficient, $a_1^{(2)}$	0.15
Occurrence probability of impulsive noise, p	0.01
Standard variances, σ_{sd1}, σ_{sr}, σ_{rd1}, and σ_{rd2}	2 dB
Means, μ_{sd1}, μ_{sr}, μ_{rd1}, and μ_{rd2}	-4 dB
Operating frequency, f	30 MHz
Exponent of attenuation factor m	0.7
Constant, b_0	9.4×10^{-3}
Constant, b_1	4.2×10^{-7}

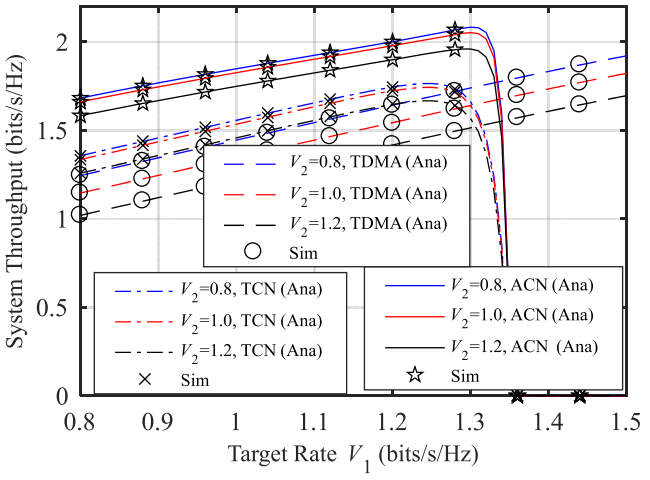

FIGURE 2. System throughput as a function of $V1$ for various $V2$.

IV. SIMUATION RESULTS

In this section, we compare the analysis results obtained in the previous Sections II and III and Monte Carlo simulations to validate its accuracy. Specially, 10^5 realizations of log-normal distributed variables are generated. Besides, let $P_r = \kappa P_s$ and $d\text{sr} = \lambda d\text{sd2}$, where κ denotes the ratio of source transmit power to relay transmit power and $\lambda \in (0,1)$ is the distance factor. Unless specified otherwise, the system parameters in the following investigations are set as Table 2, where the $V_1 = V_2 = V$.

A. SYSTEM THROUGHPUT

To begin with, we plot in Fig. 2 the system throughput with respect to target rate V_1 for different target rate V_2. Form it, we can see that each scheme's system throughput increases first as V_1 increases and our scheme always outperforms two benchmark schemes. The reason is that within this region, both users can decode its desired symbol by implementing any of the three schemes. However, since the designed scheme allows S to participate in the second phase's data transmission, additional data rates can be obtained, which results in a great enhancement in system throughput. The ACN and TCN schemes then decrease slowly with the further increase of V_1, and then rapidly drop to zero. Also, the proposed ACN scheme can achieve a higher throughput performance than the TCN scheme. The reason is that, within this region, it becomes hard for D1 and R to decode $x_1^{(1)}$ such that the success decoding probability gets smaller. However, in the proposed scheme, $x_1^{(1)}$ can be recovered at D1 during the second phase, resulting in a more reliable data reception of $x_1^{(1)}$. Besides, we can see that within in the region, the TDMA scheme keeps increasing due to mutual interference between different PLC modems does not exist.

The system throughput as a function of $a_1^{(1)}$ for different V is presented in Fig. 3. We can see that given a fixed V, the throughput achieved by our scheme equals zero before increasing quickly, because R and D1 will always fail in decoding $x_1^{(1)}$ if $\frac{R_1}{1+R_1} \leq a_1^{(1)}$, as stated in **Lemma 1-5**. The system throughput then decreases after achieving a maximal value for given V. The reason is that $a_2^{(1)}$ becomes smaller with the increase of $a_1^{(1)}$ such that the success decoding probability of $x_2^{(1)}$ at R and D2 gets smaller, resulting in a lower throughput. Moreover, the maximal value of system throughput is determined in the region of $a_1^{(1)} \in (\frac{R_1}{1+R_1}, 1)$. It is also seen that in this region, the proposed scheme can obtain a better throughput performance than two benchmark schemes.

We next show in Fig. 4 the system throughput as a function of ρ_s for different V. For a fixed V, the larger source transmit SNR, the higher system throughput. This is because the higher ρ_s can help resist to the harmful influence of noise and interference such that the success decoding probability of data symbols at each receiver increases, which enhances the system throughput. When ρ_s is large enough, both users can correctly decode the corresponding signals and accordingly the throughput achieves its maximum. Besides, with a large ρ_s, our scheme can achieve a better system performance than two benchmark schemes.

Fig. 5 shows that the system throughput as a function of κ for various V_2. The κ is the relative transmit power of R compared with that of S. For our scheme, the system throughput increases first and then decreases gradually with the increase of κ. This is because that, the relay transmit power gets lager as κ increases such that the success decoding probability of $x_2^{(1)}$ at D2 gets larger and accordingly the system throughput increases. Meanwhile, at D1, the strength of interference signal introduced by R also gets larger with the increase of κ during the second phase, which corresponds to (10). As a result, when κ is too large, the system throughput decreases gradually and tends to steady at last. It is also seen that system throughput of two benchmark schemes increases first and then tends to steady for various V_2. Since the signal from R does not affect any other modems but D2, the success decoding probability of $x_2^{(1)}$ at D2 tends to steady after achieving its maximum value when the κ is large enough.

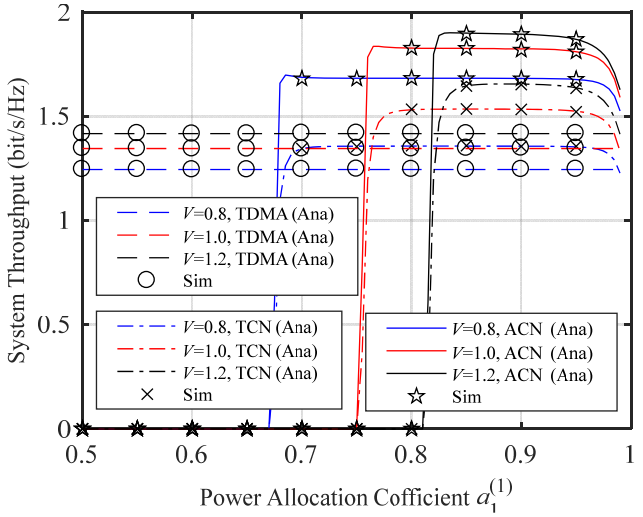

FIGURE 3. System throughput as a function of $a_1^{(1)}$ for various V.

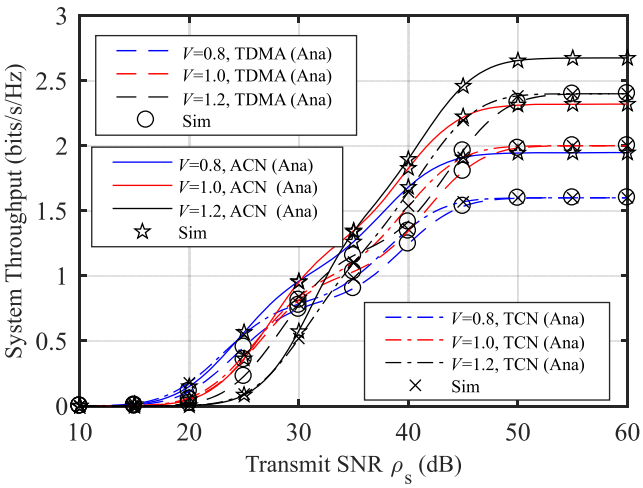

FIGURE 4. System throughput as a function of ρ_S for various V.

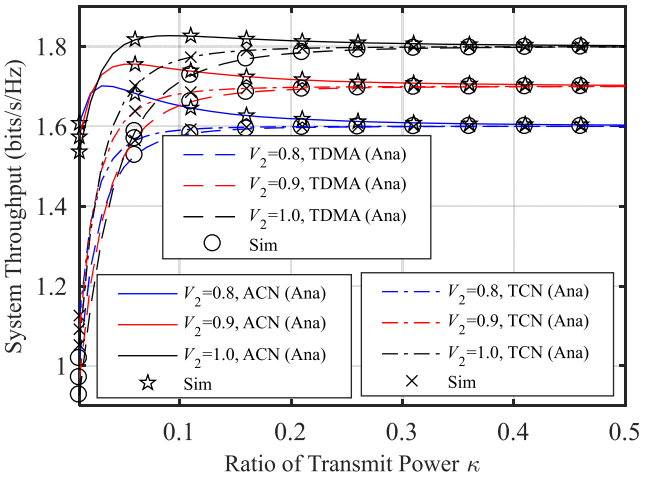

FIGURE 5. System throughput as a function of κ for various V_2 with $V_1 = 0.8$ bits/s/Hz.

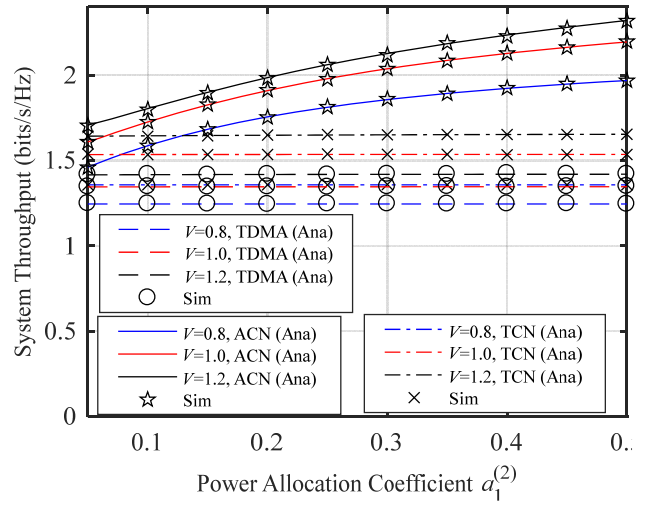

FIGURE 6. System throughput as a function of $a_1^{(2)}$ for various V.

Fig. 6 depicts that the system throughput as a function of $a_1^{(2)}$ for various V. For each given V, our scheme's throughput keeps increasing with the increase of $a_1^{(2)}$, due to the increasing of $a_1^{(2)}$ can help improve the success decoding probability of $x_1^{(2)}$ at D1. Also, it can be seen that the system throughput of the designed scheme greatly outperforms that of two benchmark schemes. The reason is that, our scheme allows R and S to participate in the second phase's data transmission or helps D1 recover $x_1^{(1)}$, which results in an additional data rates or a larger success decoding probability of $x_1^{(1)}$ at D1.

From Fig. 2 to Fig. 6, it is clear that the theoretical analysis of the system throughput closely matched the simulation results, which verifies our theoretical analysis in Section II and III.

B. MAXIMAL SYSTEM THROUGHPUT

Extensive simulations are conducted in this part to search the optimal parameters which will offer the maximal throughput.

The impact of V_1 and V_2 on system throughput is showed in Fig. 7. From it, we can see that with the increase of V_2, the system throughput increases firstly, then decreases gradually, and finally tends to a constant for each scheme. We know that the system throughput is a multiplication between the data symbol's target rate and its success decoding probability. Therefore, although the success decoding probability of $x_2^{(1)}$ at R and D2 gets smaller with the increasing V_2, the throughput will get larger if the increase of the target rate combats the decrease of the success decoding probability; otherwise, the throughput will get smaller. From low to high V_1, our scheme 's throughput achieves its maximum and respectively equals 1.68 bits/s/Hz, 1.85 bits/s/Hz and 2.00 bits/s/Hz when $V_2 = 0.84$ bits/s/Hz.

We plot in Fig. 8 the system throughput as a function of λ for variousρ_s, where $d_{sd2} = 400$ m, and $\rho_r = 30$ dB. The throughput firstly gets larger and then decreases when R approaches D2. From low to high λ, the ACN scheme's $\kappa\rho_s$ throughput reaches the maximum and equals 1.83 bits/s/Hz, 1.96 bits/s/Hz and 2.07 bits/s/Hz when λ

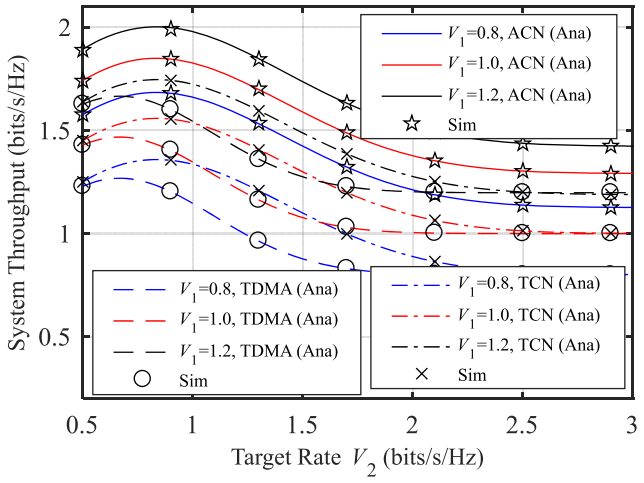

FIGURE 7. System throughput as a function of V_2 for various V_1.

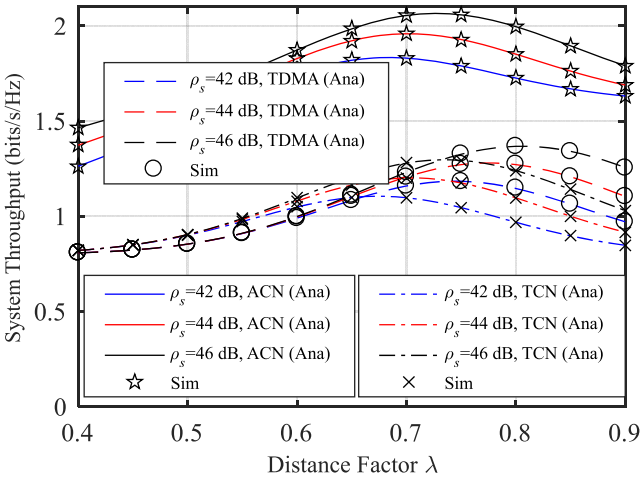

FIGURE 8. System throughput as a function of λ for various V_2 with $d_{sd2} = 400$ m, and $\rho_r = 30$dB.

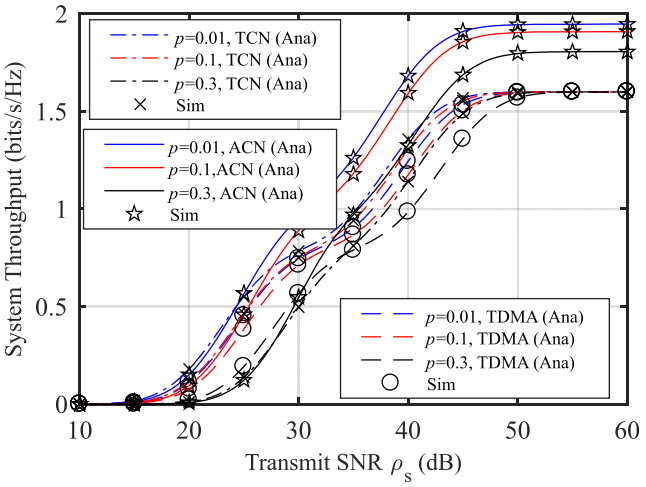

FIGURE 9. System throughput as a function of ρ_s for various p.

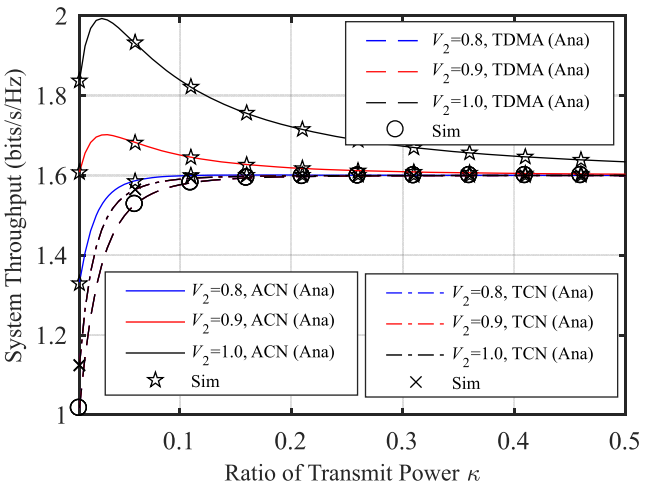

FIGURE 10. System throughput as a function of κ for various V_2 with $V_1 = 0.8$ bits/s/Hz.

respectively equals 0.68, 0.70 and 0.73. If R is located much closer to D2, the slighter channel attenuation associated with distance between R and D2 will be experienced and thus the larger success decoding probability of $x_2^{(1)}$ at D2 will be obtained, which results in an enhancement of throughput. However, the channel attenuation between S and R will be serious if λ increases further, which leads to a smaller throughput.

Fig. 9 illustrates the system throughput as a function ρ_s for different p. The variation trend of Fig. 9 is similar to that of Fig.4. From it, we can see that, in a high ρ_s region, the system throughput tends to steady and p affects the system performance than the source transmit SNR. From low to high p, the steady throughput respectively equals 1.95 bits/s/Hz, 1.91 bits/s/Hz and 1.81 bits/s/Hz. The Fig. 10 descripts the impact of κ on system performance for different V_2, which variation trend is roughly similar to that of Fig. 5. From low to high V_2, our scheme's throughput reaches its maximum and equals 1.60 bits/s/Hz, 1.70 bits/s/Hz and 1.99 bits/s/Hz when κ equals 0.3, 0.035, and 0.017, respectively.

It is worth noting that the aforementioned analytical and simulated results are based on the configuration that the overall power consumption of our scheme is at most $\frac{1}{2}(1 + a_1^{(2)})P_s + \frac{1}{2}P_r$, but that of two benchmark schemes is exactly $\frac{1}{2}(1 + a_1^{(2)})P_s + \frac{1}{2}P_r$. This means that in practice, our scheme can obtain a better throughput performance with a lower power consumption than benchmark schemes. Therefore, our scheme has potential to more efficiently reduce the EMC issues for PLC networks.

V. CONCLUSION

This paper proposes an adaptive cooperative NOMA scheme for PLC networks by introducing a negligible 1-bit feedback from the near-user. Based on the decoding status, the near-user communicates with source through an adaptively way, which switches between a direct and a cooperative data transmission mode. This results in an enhancement of the system throughput and a more reliable data reception at the near-user. We analyze the system throughput under different data transmission modes and reveal the impacts of key system parameters. Finally, simulation results validate our

theoretical analysis, and show that compared with two benchmark schemes, our scheme can obtain a better throughput performance with a lower power consumption and reduce the EMC issues for PLC networks more efficiently.

APPENDIX A

By rearranging (24) and (30), $\Pr\{A, D\}$ and $\Pr\{A\overline{D}\}$ can be respectively derived in (61) and (62), as shown at the bottom of this page, where the indicator variables $1_{\Im_0}$ and $1_{\Im_1}$ are respectively given in **Lemma 1** and **Lemma 2**. Using some basic mathematical manipulations, we can further calculate them as

$$\Pr\{A, D\} = 1_{\Im_0} \int_{I_0} f_{|h_{\mathrm{sd1}}|^2}(x) \Pr\left\{|h_{\mathrm{rd1}}|^2 \le \Phi(x)\right\} \mathrm{d}x, \quad (56)$$

and

$$\Pr\left\{A, \overline{D}\right\} = 1_{\Im_0} \underbrace{\int_{I_0} f_{|h_{\mathrm{sd1}}|^2}(x) \Pr\left\{|h_{\mathrm{rd1}}|^2 > \Phi(x)\right\} \mathrm{d}x}_{\phi_{11}} + 1_{\Im_1} \underbrace{\int_{I_1} f_{|h_{\mathrm{sd1}}|^2}(x) \mathrm{d}x}_{\phi_{12}}, \quad (57)$$

where the integral interval I_0 and the variable $\Phi(x)$ are given in **Lemma 1**, the integral intervalI_1 is given in **Lemma 2**. We know that the variables $|h_{\mathrm{sd1}}|^2$ and $|h_{\mathrm{rd1}}|^2$ are log-normal distributed with parameters $|h_{\mathrm{sd1}}|^2 \sim \ln N\left(2\mu_{\mathrm{sd1}}, (2\sigma_{\mathrm{sd1}})^2\right)$ and $|h_{\mathrm{rd1}}|^2 \sim \ln N\left(2\mu_{\mathrm{rd1}}, (2\sigma_{\mathrm{rd1}})^2\right)$, respectively, and $f_{|h_{\mathrm{sd1}}|^2}(x)$ in (56) and (57) is the PDF of $|h_{\mathrm{sd1}}|^2$. Using (25)-(27), we can finally derive the probability of $\Pr\{A, D\}$ as (29) and the terms ϕ_{11} and ϕ_{12} in $\Pr\{A\overline{D}$ can be derived as (31) and (32).

APPENDIX B

In (37), (41) and (45), when $\Gamma\left(|h_{\mathrm{sd1}}|^2\right) < R_2$, we have $a_1^{(1)} < \frac{1}{R_2+1}$, $|h_{\mathrm{sd1}}|^2 < \frac{R_2}{A_{\mathrm{sd1}}^2\left(a_2^{(1)} - a_1^{(1)} R_2\right)\rho_s}$ or $a_1^{(1)} \ge \frac{1}{R_2+1}$, $|h_{\mathrm{sd1}}|^2 \ge 0$, while $\Gamma\left(|h_{\mathrm{sd1}}|^2\right) \ge R_2$, we have $a_1^{(1)} < \frac{1}{R_2+1}$, $|h_{\mathrm{sd1}}|^2 \ge \frac{R_2}{A_{\mathrm{sd1}}^2\left(a_2^{(1)} - a_1^{(1)} R_2\right)\rho_s}$. Therefore, the expressions of $\Pr\left\{\overline{A}, E, F\right\}$, $\Pr\{\overline{A}E\overline{F}\}$ and $\Pr\{\overline{AE}\}$ can be further respectively derived in (63)–(65), as shown at the top of the next page, where the indicator variables $1_{\Im_2}, 1_{\Im_3}, 1_{\Im_4}, 1_{\Im_5}, 1_{\Im_6} 1_{\Im_7}$ and $1_{\Im_8}, 1_{\Im_9}$ are respectively given in **Lemma 3**, **Lemma 4** and **Lemma 5**. The terms ϕ_{21}, ϕ_{22},and ϕ_{23}consist in $\Pr\left\{\overline{A}, E, F\right\}$, the terms ϕ_{31}, ϕ_{32}, and ϕ_{33} consist in $\Pr\{\overline{A}E\overline{F}\}$, and the terms ϕ_{41} and ϕ_{42} consist in $\Pr\{\overline{AE}\}$. By performing some variable substitutions, these probabilities can be further respectively calculated as

$$\begin{aligned}\Pr\left\{\overline{A}, E, F\right\} = {} & 1_{\Im_2} \underbrace{\int_{I_2} f_{|h_{\mathrm{sd1}}|^2}(x) \Pr\left\{|h_{\mathrm{rd1}}|^2 \ge \Omega(x)\right\} \mathrm{d}x}_{\phi_{21}} \\ & + 1_{\Im_3} \underbrace{\int_{I_3} f_{|h_{\mathrm{sd1}}|^2}(x) \Pr\left\{|h_{\mathrm{rd1}}|^2 \ge \Omega(x)\right\} \mathrm{d}x}_{\phi_{22}} \\ & + 1_{\Im_4} \underbrace{\int_{I_4} f_{|h_{\mathrm{sd1}}|^2}(x) \mathrm{d}x}_{\phi_{23}}, \end{aligned} \quad (58)$$

$$\begin{aligned}\Pr\left\{\overline{A}, E, \overline{F}\right\} = {} & 1_{\Im_5} \underbrace{\int_{I_5} f_{|h_{\mathrm{sd1}}|^2}(x) \Pr\left\{|h_{\mathrm{rd1}}|^2 \ge \Omega(x)\right\} \mathrm{d}x}_{\phi_{31}} \\ & + 1_{\Im_6} \underbrace{\int_{I_6} f_{|h_{\mathrm{sd1}}|^2}(x) \Pr\left\{|h_{\mathrm{rd1}}|^2 \ge \Omega(x)\right\} \mathrm{d}x}_{\phi_{32}} \\ & + 1_{\Im_7} \underbrace{\int_{I_7} f_{|h_{\mathrm{sd1}}|^2}(x) \mathrm{d}x}_{\phi_{33}}, \end{aligned} \quad (59)$$

and

$$\begin{aligned}\Pr\left\{\overline{A}, \overline{E}\right\} = {} & \underbrace{1_{\Im_8} \int_{I_8} f_{|h_{\mathrm{sd1}}|^2}(x) \Pr\left\{|h_{\mathrm{rd1}}|^2 < \Omega(x)\right\} \mathrm{d}x}_{\phi_{41}} \\ & + \underbrace{1_{\Im_9} \int_{I_9} f_{|h_{\mathrm{sd1}}|^2}(x) \Pr\left\{|h_{\mathrm{rd1}}|^2 < \Omega(x)\right\} \mathrm{d}x}_{\phi_{42}} \end{aligned} \quad (60)$$

$$\begin{aligned}&\Pr\{A, D\} \\ &= 1_{\Im_0} \Pr\left\{|h_{\mathrm{sd1}}|^2 \ge \frac{R_1}{A_{\mathrm{sd1}}^2\left(a_1^{(1)} - a_2^{(1)} R_1\right)\rho_s}, |h_{\mathrm{rd1}}|^2 \le \frac{|h_{\mathrm{sd1}}|^2 A_{\mathrm{sd1}}^2 a_1^{(2)} \rho_s - R_1}{A_{\mathrm{rd1}}^2 \rho_r R_1}, |h_{\mathrm{sd1}}|^2 \ge \frac{R_1}{A_{\mathrm{sd1}}^2 a_1^{(2)} \rho_s}\right\} \end{aligned} \quad (61)$$

$$\begin{aligned}&\Pr\left\{A, \overline{D}\right\} \\ &= \underbrace{1_{\Im_0} \Pr\left\{|h_{\mathrm{sd1}}|^2 \ge \frac{R_1}{A_{\mathrm{sd1}}^2\left(a_1^{(1)} - a_2^{(1)} R_1\right)\rho_s}, |h_{\mathrm{rd1}}|^2 > \frac{|h_{\mathrm{sd1}}|^2 A_{\mathrm{sd1}}^2 a_1^{(2)} \rho_s - R_1}{A_{\mathrm{rd1}}^2 \rho_r R_1}, |h_{\mathrm{sd1}}|^2 \ge \frac{R_1}{A_{\mathrm{sd1}}^2 a_1^{(2)} \rho_s}\right\}}_{\phi_{11}} \\ &\quad + \underbrace{1_{\Im_1} \Pr\left\{|h_{\mathrm{sd1}}|^2 \ge \frac{R_1}{A_{\mathrm{sd1}}^2\left(a_1^{(1)} - a_2^{(1)} R_1\right)\rho_s}, |h_{\mathrm{sd1}}|^2 < \frac{R_1}{A_{\mathrm{sd1}}^2 a_1^{(2)} \rho_s}\right\}}_{\phi_{12}} \end{aligned} \quad (62)$$

$$\begin{aligned}
&\Pr\left\{\overline{A}, E, F\right\} \\
&= 1_{\Im_2} \underbrace{\Pr\left\{|h_{\mathrm{sd1}}|^2 < \frac{R_1}{A_{\mathrm{sd1}}^2\left(a_1^{(1)} - a_2^{(1)}R_1\right)\rho_s}, |h_{\mathrm{rd1}}|^2 \geq \frac{R_2 - \Gamma\left(|h_{\mathrm{sd1}}|^2\right)}{A_{\mathrm{rd1}}^2 P_r}, |h_{\mathrm{sd1}}|^2 < \frac{R_2}{A_{\mathrm{sd1}}^2\left(a_2^{(1)} - a_1^{(1)}R_2\right)\rho_s}, h_{\mathrm{sd1}}^2 \geq \frac{R_1}{A_{\mathrm{sd1}}^2 a_1^{(1)}\rho_s}\right\}}_{\phi_{21}} \\
&\quad + 1_{\Im_3} \underbrace{\Pr\left\{|h_{\mathrm{sd1}}|^2 < \frac{R_1}{A_{\mathrm{sd1}}^2\left(a_1^{(1)} - a_2^{(1)}R_1\right)\rho_s}, |h_{\mathrm{rd1}}|^2 \geq \frac{R_2 - \Gamma\left(|h_{\mathrm{sd1}}|^2\right)}{A_{\mathrm{rd1}}^2 P_r}, h_{\mathrm{sd1}}^2 \geq \frac{R_1}{A_{\mathrm{sd1}}^2 a_1^{(1)}\rho_s}\right\}}_{\phi_{22}} \\
&\quad + 1_{\Im_4} \underbrace{\Pr\left\{|h_{\mathrm{sd1}}|^2 < \frac{R_1}{A_{\mathrm{sd1}}^2\left(a_1^{(1)} - a_2^{(1)}R_1\right)\rho_s}, |h_{\mathrm{sd1}}|^2 \geq \frac{R_2}{A_{\mathrm{sd1}}^2\left(a_2^{(1)} - a_1^{(1)}R_2\right)\rho_s}, h_{\mathrm{sd1}}^2 \geq \frac{R_1}{A_{\mathrm{sd1}}^2 a_1^{(1)}\rho_s}\right\}}_{\phi_{23}}
\end{aligned} \tag{63}$$

$$\begin{aligned}
&\Pr\left\{\overline{A}, E, \overline{F}\right\} \\
&= 1_{\Im_5} \underbrace{\Pr\left\{|h_{\mathrm{sd1}}|^2 < \frac{R_1}{A_{\mathrm{sd1}}^2\left(a_1^{(1)} - a_2^{(1)}R_1\right)\rho_s}, |h_{\mathrm{rd1}}|^2 \geq \frac{R_2 - \Gamma\left(|h_{\mathrm{sd1}}|^2\right)}{A_{\mathrm{rd1}}^2 P_r}, |h_{\mathrm{sd1}}|^2 < \frac{R_2}{A_{\mathrm{sd1}}^2\left(a_2^{(1)} - a_1^{(1)}R_2\right)\rho_s}, h_{\mathrm{sd1}}^2 < \frac{R_1}{A_{\mathrm{sd1}}^2 a_1^{(1)}\rho_s}\right\}}_{\phi_{31}} \\
&\quad + 1_{\Im_6} \underbrace{\Pr\left\{|h_{\mathrm{sd1}}|^2 < \frac{R_1}{A_{\mathrm{sd1}}^2\left(a_1^{(1)} - a_2^{(1)}R_1\right)\rho_s}, |h_{\mathrm{rd1}}|^2 \geq \frac{R_2 - \Gamma\left(|h_{\mathrm{sd1}}|^2\right)}{A_{\mathrm{rd1}}^2 P_r}, h_{\mathrm{sd1}}^2 < \frac{R_1}{A_{\mathrm{sd1}}^2 a_1^{(1)}\rho_s}\right\}}_{\phi_{32}} \\
&\quad + 1_{\Im_7} \underbrace{\Pr\left\{|h_{\mathrm{sd1}}|^2 < \frac{R_1}{A_{\mathrm{sd1}}^2\left(a_1^{(1)} - a_2^{(1)}R_1\right)\rho_s}, |h_{\mathrm{sd1}}|^2 \geq \frac{R_2}{A_{\mathrm{sd1}}^2\left(a_2^{(1)} - a_1^{(1)}R_2\right)\rho_s}, h_{\mathrm{sd1}}^2 < \frac{R_1}{A_{\mathrm{sd1}}^2 a_1^{(1)}\rho_s}\right\}}_{\phi_{33}}
\end{aligned} \tag{64}$$

$$\begin{aligned}
&\Pr\left\{\overline{A}, \overline{E}\right\} \\
&= 1_{\Im_8} \underbrace{\Pr\left\{|h_{\mathrm{sd1}}|^2 < \frac{R_1}{A_{\mathrm{sd1}}^2\left(a_1^{(1)} - a_2^{(1)}R_1\right)\rho_s}, |h_{\mathrm{rd1}}|^2 < \frac{R_2 - \Gamma\left(|h_{\mathrm{sd1}}|^2\right)}{A_{\mathrm{rd1}}^2 P_r}, |h_{\mathrm{sd1}}|^2 < \frac{R_2}{A_{\mathrm{sd1}}^2\left(a_2^{(1)} - a_1^{(1)}R_2\right)\rho_s}\right\}}_{\phi_{41}} \\
&\quad + 1_{\Im_9} \underbrace{\Pr\left\{|h_{\mathrm{sd1}}|^2 < \frac{R_1}{A_{\mathrm{sd1}}^2\left(a_1^{(1)} - a_2^{(1)}R_1\right)\rho_s}, |h_{\mathrm{rd1}}|^2 < \frac{R_2 - \Gamma\left(|h_{\mathrm{sd1}}|^2\right)}{A_{\mathrm{rd1}}^2 P_r}\right\}}_{\phi_{42}}
\end{aligned} \tag{65}$$

where the integral intervals $I_4 = (\max(\beta_2, \beta_3), \beta_0)$, and $I_7 = (\beta_2, \min(\beta_0, \beta_3))$. The integral intervals I_2 and I_3 are given in **Lemma 3**, the integral intervals I_5 and I_6 are given in **Lemma 4**, and integral intervals I_8 and I_9 are given in **Lemma 5**. The variable $\Omega(x)$ in (58)-(60) is given in **Lemma 3**. Using the properties of the log-normal distributed variables $|h_{\mathrm{sd1}}|^2$ and $|h_{\mathrm{rd1}}|^2$, the terms ϕ_{21}, ϕ_{22}, and ϕ_{23} can be obtained as (38), (39) and (40), the terms ϕ_{31}, ϕ_{32}, and ϕ_{33} can be derived as (42), (43) and (44), and the terms ϕ_{41} and ϕ_{42} can be calculated as (46), (47) and (48).

REFERENCES

[1] Z. Khan, J. J. Lehtomaki, S. I. Iellamo, R. Vuohtoniemi, E. Hossain, and Z. Han, "IoT connectivity in radar bands: A shared access model based on spectrum measurements," *IEEE Commun. Mag.*, vol. 55, no. 2, pp. 88–96, Feb. 2017.

[2] Y. Qian, J. Yan, H. Guan, J. Li, X. Zhou, S. Guo, and D. N. K. Jayakody, "Design of hybrid wireless and power line sensor networks with dual-interface relay in IoT," *IEEE Internet Things J.*, vol. 6, no. 1, pp. 239–249, Feb. 2019. doi: 10.1109/JIOT.2017.2725451.

[3] Y.-W. Qian, M. Tian, X. Jian, H.-J. Song, S. Feng, and J. Li, "Performance analysis for a two-way relaying power line network with analog network coding," *Frontiers Inf. Technol. Electron. Eng.*, vol. 16, no. 10, pp. 892–898, 2015.

[4] K. M. Rabie, B. Adebisi, H. Gacanin, and S. Yarkan, "Energy-per-bit performance analysis of relay-assisted power line communication systems," *IEEE Trans. Green Commun. Netw.*, vol. 2, no. 2, pp. 360–368, Jun. 2018.

[5] K. M. Rabie and E. Alsusa, "Effective noise cancellation using single carrier FDMA transmission in power-line channels," *IEEE Trans. Power Del.*, vol. 29, no. 5, pp. 2110–2117, Oct. 2014.

[6] K. M. Rabie and E. Alsusae, "On improving communication robustness in PLC systems for more reliable smart grid applications," *IEEE Trans. Smart Grid*, vol. 6, no. 6, pp. 2746–2756, Nov. 2015.

[7] M. Nassar, J. Lin, Y. Mortazavi, A. Dabak, I. H. Kim, and B. Evans, "Local utility power line communications in the 3–500 kHz band: Channel impairments, noise, and standards," *IEEE Signal Process. Mag.*, vol. 29, no. 5, pp. 116–127, Sep. 2012.

[8] B. Adebisi, J. Stott, and B. Honary, "Experimental study of the interference caused by PLC transmission on HF bands," in *Proc. 10th IET Int. Conf. Ionospheric Radio Syst. Techn. (IRST)*, Beijing, China, 2006, pp. 326–330.
[9] X. Cheng, R. Cao, and L. Yang, "Relay-aided amplify-and-forward power-line communications," *IEEE Trans. Smart Grid*, vol. 4, no. 1, pp. 265–272, Mar. 2013.
[10] A. Salem, K. M. Rabie, K. A. Hamdi, E. Alsusa, and A. M. Tonello, "Physical layer security of cooperative relaying power-line communication systems," in *Proc. Int. Symp. Power Line Commun. Appl. (ISPLC)*, Bottrop, Germany, Mar. 2016, pp. 185–189.
[11] J. Valencia, T. R. Oliveira, and M. V. Ribeiro, "Cooperative power line communication: Analysis of brazilian in-home channels," in *Proc. 18th IEEE Int. Symp. Power Line Commun. Appl.*, Glasgow, U.K., 2014, pp. 301–305.
[12] S. Ezzine, F. Abdelkefi, J. P. Cances, V. Meghdadi, and A. Bouallegue, "Capacity analysis of an OFDM-based two-hops relaying PLC systems," in *Proc. IEEE 81st Veh. Technol. Conf. (VTC Spring)*, Glasgow, U.K., May 2015, pp. 1–5.
[13] M. S. P. Facina, H. A. Latchman, H. V. Poor, and M. V. Ribeiro, "Cooperative in-home power line communication: Analyses based on a measurement campaign," *IEEE Trans. Commun.*, vol. 64, no. 2, pp. 778–789, Feb. 2016.
[14] K. M. Rabie, B. Adebisi, A. M. Tonello, and G. Nauryzbayev, "For more energy-efficient dual-hop DF relaying power-line communication systems," *IEEE Syst. J.*, vol. 12, no. 2, pp. 2005–2016, Jun. 2018.
[15] K. M. Rabie and B. Adebisi, "Enhanced amplify-and-forward relaying in non-Gaussian PLC networks," *IEEE Access*, vol. 5, pp. 4087–4094, 2017.
[16] Y. Qian, J. Li, Y. Zhang, and D. N. K. Jayakody, "Performance analysis of an opportunistic relaying power line communication systems," *IEEE Syst. J.*, vol. 12, no. 4, pp. 3865–3868, Dec. 2018.
[17] R. Jiao, L. Dai, J. Zhang, R. MacKenzie, and M. Hao, "On the performance of NOMA-based cooperative relaying systems over Rician fading channels," *IEEE Trans. Veh. Technol.*, vol. 66, no. 12, pp. 11409–11413, Dec. 2017.
[18] O. Abbasi, A. Ebrahimi, and N. Mokari, "NOMA inspired cooperative relaying system using an AF relay," *IEEE Wireless Commun. Lett.*, vol. 8, no. 1, pp. 261–264, Feb. 2019. doi: 10.1109/LWC.2018.2869592.
[19] K. M. Rabie, B. Adebisi, E. H. Yousif, H. Gacanin, and A. M. Tonello, "A comparison between orthogonal and non-orthogonal multiple access in cooperative relaying power line communication systems," *IEEE Access*, vol. 5, pp. 10118–10129, 2017.
[20] K. M. Rabie, B. Adebisi, A. M. Tonello, S. Yarkan, and M. Ijaz, "Two-stage non-orthogonal multiple access over power line communication channels," *IEEE Access*, vol. 6, pp. 17368–17376, 2018.
[21] X. Liu, L. Li, Z. Li, X. Chen, T. Fernando, H. H.-C. Iu, and G. He, "Event-trigger particle filter for smart grids with limited communication bandwidth infrastructure," *IEEE Trans. Smart Grid*, vol. 9, no. 6, pp. 6918–6928, Nov. 2018.
[22] S. Li, L. Li, Z. Li, X. Chen, T. Fernando, H.-H. Iu, G. He, Q. Wang, and X. Liu, "Event-trigger heterogeneous nonlinear filter for wide-area measurement systems in power grid," *IEEE Trans. Smart Grid*, vol. 10, no. 3, pp. 2752–2764, Feb. 2018. doi: 10.1109/TSG.2018.2810224.
[23] X. Liang, Y. Wu, D. W. K. Ng, Y. Zuo, S. Jin, and H. Zhu, "Outage performance for cooperative NOMA transmission with an AF relay," *IEEE Commun. Lett.*, vol. 21, no. 11, pp. 2428–2431, Nov. 2017.
[24] J.-B. Kim and I.-H. Lee, "Non-orthogonal multiple access in coordinated direct and relay transmission," *IEEE Commun. Lett.*, vol. 19, no. 11, pp. 2037–2040, Nov. 2015.
[25] C. Zhong and Z. Zhang, "Non-orthogonal multiple access with cooperative full-duplex relaying," *IEEE Commun. Lett.*, vol. 20, no. 12, pp. 2478–2481, Dec. 2016.
[26] T. M. C. Chu and H.-J. Zepernick, "Performance of a non-orthogonal multiple access system with full-duplex relaying," *IEEE Commun. Lett.*, vol. 22, no. 10, pp. 2084–2087, Oct. 2018.
[27] S. Efazati and P. Azmi, "Cross layer power allocation for selection relaying and incremental relaying protocols over single relay networks," *IEEE Trans. Wireless Commun.*, vol. 15, no. 7, pp. 4598–4610, Jul. 2016.
[28] K. M. Rabie, B. Adebisi, and H. Gacanin, "Outage probability and energy efficiency of DF relaying power line communication networks: Cooperative and non-cooperative," in *Proc. IEEE Int. Conf. Commun. (ICC)*, Paris, France, May 2017, pp. 1–6.
[29] A. Dubey and R. K. Mallik, "PLC system performance with AF relaying," *IEEE Trans. Commun.*, vol. 63, no. 6, pp. 2337–2345, Jun. 2015.
[30] A. Dubey, R. K. Mallik, and R. Schober, "Performance analysis of a multi-hop power line communication system over log-normal fading in presence of impulsive noise," *IET Commun.*, vol. 9, no. 1, pp. 1–9, Jan. 2015.
[31] Z. Ding, H. Dai, and H. V. Poor, "Relay selection for cooperative NOMA," *IEEE Wireless Commun. Lett.*, vol. 5, no. 4, pp. 416–419, Aug. 2016.
[32] M. Antoniali, F. Versolatto, and A. M. Tonello, "An experimental characterization of the PLC noise at the source," *IEEE Trans. Power Del.*, vol. 31, no. 3, pp. 1068–1075, Jun. 2016.

HONGHONG PU (S'19) was born in Anhui, China, in 1992. She received the B.S. degree in electrical engineering and automation from the Luoyang Institute of Science and Technology, Luoyang, China, in 2015, and the M.S. degree in control engineering from the Harbin Institute of Technology, Harbin, China, in 2017, where she is currently pursuing the Ph.D. degree in electrical engineering. Her research interests include power line communication and its relaying methods, and MAC protocols.

XIAOSHENG LIU (M'14) was born in Qiqihar, Heilongjiang, China, in 1966. He received the B.S. and M.S. degrees in electrical engineering and the Ph.D. degree in mechatronics engineering from the Harbin Institute of Technology, Harbin, China, in 1988, 1993, and 1999, respectively, where he has been a Professor with the Department of Electrical Engineering, since 2006. His current research interests include power line communication and its routing methods, communication networks and control technology, and information and communication of smart grids.

SHU ZHANG (S'15) was born in Heilongjiang, China, in 1988. He received the B.S. degree in electrical engineering from the Civil Aviation University of China, Tianjin, China, in 2012, and the M.S. degree in electrical engineering from the Harbin Institute of Technology, Harbin, China, in 2014, where he is currently pursuing the Ph.D. degree in power electronics and electrical drives with the School of Electrical Engineering and Automation. His research interests include LED drivers and single stage ac/dc converters.

DIANGUO XU (M'97–SM'12–F'17) received the B.S. degree in control engineering from the Harbin Engineering University, Harbin, China, in 1982, and the M.S. and Ph.D. degrees in electrical engineering from the Harbin Institute of Technology (HIT), Harbin, China, in 1984 and 1989, respectively. In 1984, he joined the Department of Electrical Engineering, HIT, as an Assistant Professor, where he has been a Professor with the Department of Electrical Engineering, since 1994. He was the Dean of the School of Electrical Engineering and Automation, HIT, from 2000 to 2010. He is currently the Vice President of HIT. He has published over 600 technical papers. His research interests include renewable energy generation technology, power quality mitigation, sensorless vector controlled motor drives, and high-performance PMSM servo systems. He serves as a Chairman of the IEEE Harbin Section. He is currently an Associate Editor of the IEEE TRANSACTIONS ON INDUSTRIAL ELECTRONICS and the IEEE JOURNAL OF EMERGING AND SELECTED TOPICS IN POWER ELECTRONICS.